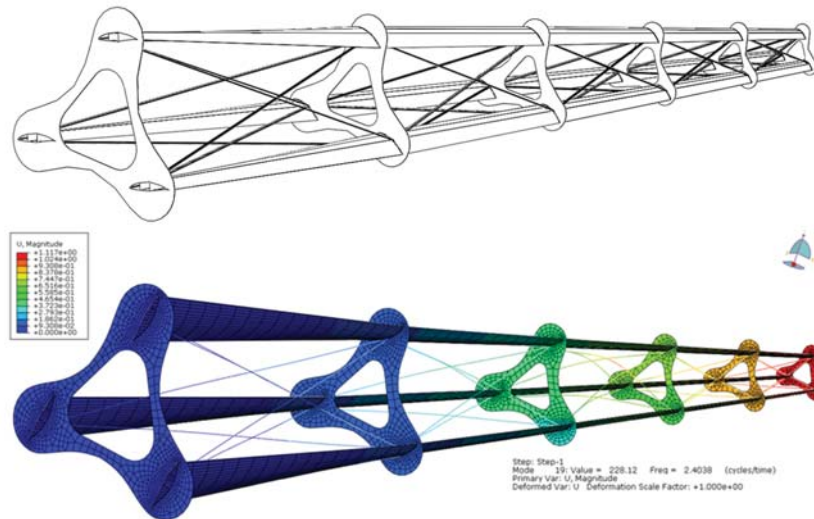




LUND
UNIVERSITY



STRUCTURAL ANALYSIS OF TRUSS CONSTRUCTION FOR WIND TURBINE BLADES

BJÖRN WEDDIG

Structural
Mechanics

Master's Dissertation

DEPARTMENT OF CONSTRUCTION SCIENCES
DIVISION OF STRUCTURAL MECHANICS

ISRN LUTVDG/TVSM--16/5215--SE (1-69) | ISSN 0281-6679

MASTER'S DISSERTATION

STRUCTURAL ANALYSIS OF TRUSS CONSTRUCTION FOR WIND TURBINE BLADES

BJÖRN WEDDIG

Supervisor: Professor **KENT PERSSON**, Div. of Structural Mechanics, LTH.

Examiner: Professor **PER-ERIK AUSTRELL**, Div. of Structural Mechanics, LTH.

Copyright © 2016 Division of Structural Mechanics,
Faculty of Engineering LTH, Lund University, Sweden.

Printed by Media-Tryck LU, Lund, Sweden, May 2016 (*PI*).

For information, address:

Division of Structural Mechanics,
Faculty of Engineering LTH, Lund University, Box 118, SE-221 00 Lund, Sweden.

Homepage: www.byggmek.lth.se

Abstract

The usage of wind turbines during the latest years has grown substantially and are becoming an increasingly important source of renewable energy, as many countries are trying to reduce their reliance on fossil fuels. In order to increase the effect of the wind turbines the length of the blades has been increased, which has also led to an increase of the cross-section dimensions. This has led to making the weight of the blade a more dominating load. Therefore, it is of great interest to reduce the weight of wind turbine blades to continue constructing longer blades. To accomplish this Winfoor are developing a wind turbine blade that combines traditional horizontal-axis wind turbine (HAWT), with a truss system containing truss bars and a plate connected to the blades. Winfoor has the ambition to evolve the wind blade industry by modify the shape of a HAWT blade into a Triblade. The results and conclusions form this thesis are one of many things that has to be taken into account when the final design is developed.

As the truss bars are long and slender, the bars that are being compressed are more likely to buckle. The structural response of a dynamic load applied to the structure was also studied in this thesis.

Identification and evaluation of the variables, such as Young's module, influence on the load capacity was computed with non-linear numerical analysis. In order to find a design proposal containing both section dimensions and material properties was two parameter studies completed. In structural design, the load capacity was often evaluated using finite element method (FEM). This thesis includes non-linear FE analysis, which considers large deformations.

The blades structural dynamic response was evaluated using both modal, and frequency response analysis. Additionally are the response of an impulse studied using full transient analysis.

The main conclusion from this thesis where that buckling truss bars are problematic when an impulse was added to the structure. The impulse created from the tower passage was big enough to change the buckling mode of the truss bar. This generates a great variation in stresses for these truss bars, which cause it to that fatigue, damage, and this may decrease its life span.

An additionally conclusion was that the eigenfrequency for each truss bar should not overlap with the eigenfrequency for the global bending mode of the Triblade.

Keywords:

Wind turbine blade, FRP, Truss system, Instability, Buckling, Non-Linear, Eigenvalue problem, Frequency response analysis, Transient dynamic response

Preface

This master dissertation was carried out for the Division of Structural Mechanics at Lund University Faculty of Engineering (LTH) and this work marks the end of my Master's degree in Structural and Civil engineering

I would like to express my gratitude to my supervisor Ph.D. Kent Persson who gave me support throughout this work by always being available helpful when I needed guidance. I would also like to thank Rikard Berthilsson and all colleagues at Winfoor.

This thesis is the end five year of studies in Lund and I would like to thank my family and friends for your support during my education.

Lund, May 2016.

Björn Weddig

Table of Content

Abstract	6
Preface	8
Table of content	9
1 Introduction	5
1.1 Background	5
1.2 Objective and Method	6
1.3 Limitations	7
1.4 Outline of Thesis	7
2 Wind Turbine Blades	8
2.1 Fiber-reinforced polymers	8
2.2 Wind Turbine Blade Design	10
2.2.1 Structural parts	10
2.3 Triblade Geometric	11
2.3.1 Blades	11
2.3.2 Plates	12
2.3.3 Truss Bars	13
2.3.4 Truss System	13
3 Theory	15
3.1 Finite Element Method	15
3.1.1 Element Types	15
3.2 Buckling	17
3.2.1 Geometric Nonlinear analysis	17
3.3 Structural Dynamics	17
3.3.1 Natural Vibration Frequencies and Modes	17
3.3.2 Full Transient Dynamic Response	19
3.3.3 Frequency Response Analysis	19
3.3.4 Damping in Structures	20
4 Finite Element Method Model	22
4.1 Introduction	22
4.2 Mesh and Simplifications	22
4.2.1 Plates	22
4.2.2 Truss Bars	23

4.2.3	Blades	23
4.3	Material and Cross-Sections Properties	24
4.4	Boundary condition	25
4.5	Static Pressure Load	25
4.5.1	Pressure Distribution over the Wing Profile	26
4.5.2	Application of Load to Model	29
4.6	Dynamic load	32
4.6.1	Undisturbed Tower-Flow	32
4.6.2	Connection between velocity and force	34
4.6.3	Data for impulse	34
4.6.4	Damping Coefficients	37
5	Designing Sections of Triblade	38
5.1	Chapter Abstract	38
5.2	Objective	38
5.3	Method	38
5.4	Results and Analysis	39
5.4.1	Parametric Studies of Varying the Young's module	39
5.4.2	Section Dimensions	46
6	Dynamic analysis	50
6.1	Chapter Abstract	50
6.2	Objective	50
6.3	Method	50
6.4	Eigenmodes and Eigenfrequencies	51
6.4.1	Results Eigenfrequencies Undeformed Model	51
6.4.2	Results Model 2 Pre-loaded Structure	56
6.4.3	Conclusions – Modal Analysis	59
6.5	Frequency Response Function	59
6.5.1	Results Model 1 – Undeformed Model	60
6.5.2	Results Model 2 – Deformed model	61
6.5.3	Conclusions	62
6.6	Full Transient Dynamic Response	63
6.6.1	Full transient dynamic response	64
6.6.2	Model 1 – Undeformed Model	64
6.6.3	Model 2 – Deformed Model	65
6.6.4	Conclusions	66
7	Discussion and Future Work	67
8	References	68

1 Introduction

1.1 Background

The usage of wind turbines has during the latest years grown substantially and are becoming an increasingly important source of energy as many countries are trying to reduce their reliance on fossil fuels. In order to increase the power of the wind turbines the length of the blades has been increased, which has also led to an increase of the cross-sections dimensions. This has led to that the dead load of the blade a more dominating load. Therefore, it is of great interest to reduce the weight of wind turbine blades to continue constructing longer blades.

To minimize the weight and increase the capacity of a wind turbine, Winfoo have started to develop a prototype of a Triblade. A Triblade, will have three blades arranged in a triangular configuration. Six plates disposed transversely will then hold the blades together. The structure is reinforced with streamlined truss bars arranged diagonally. Combined together with the plates, this creates a truss structure as can be seen in the figure below.

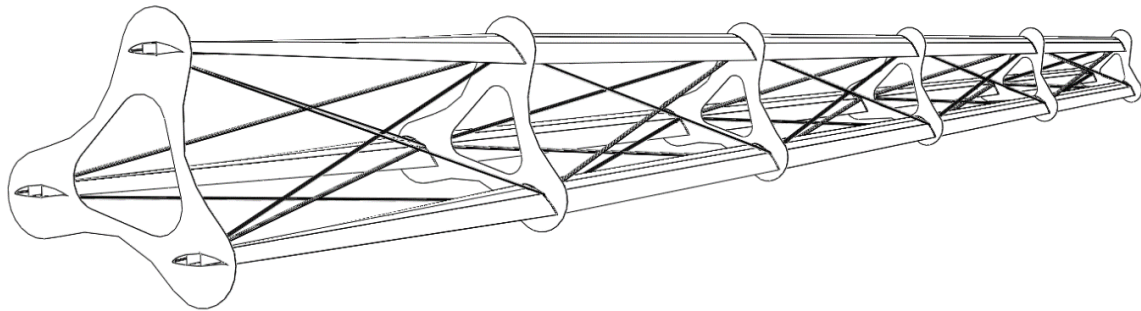


Figure 1.1: Triblade

The two most common material used in modern wind turbines are glass fiber reinforced polymers (GFRP), and carbon fiber reinforced polymers (CFRP). Both of these materials combines a high stiffness and a low density in comparison to other materials and additionally has a good fatigue resistance. Both of these materials are used in the Triblade in order to create a lightweight structure.

Since the truss bars are long and slender, the bars that are being compressed are more likely to buckle. The behavior of the structure after the truss bars have buckled will be explored more in this thesis.

The load applied to the structure is a dynamic wind load and it is also important to find the dynamic response of the structure for certain frequencies. This thesis will focus on the buckling behavior and the dynamic response of the Triblade structure that this.

In previous student internships at Winfoor a CAD model has been created and a design proposal has been optimized from a static linear calculation. This CAD model is adopted to create a finite element model that will be used in the static and dynamic analyses.

1.2 Objective and Method

The objective of this master thesis is to develop a model that can be used for investigating the buckling and the dynamic response of a Triblade. The purpose of the dynamic analysis was to find the main natural frequencies of the structure and from that find design criteria that can be useful in the future development of the design.

This thesis will also provide an overview of how the model's section properties was designed by calculating the static response when nonlinearity geometric is included this is also called buckling analysis. By including the nonlinearities, it is possible to calculate the global response of the structure after the local buckling are occurring in the truss bars. This analysis gives the magnitude of the load (also called critical buckling load) when a global buckling mode is occurring that makes the whole structure unstable.

A parametric study was completed in order to identify different variables influence on the load capacity. The investigated variables are the Young's modulus and the section thickness for the different parts.

The objective of the dynamic response was to find how the truss structure is responding together with the blades for dynamic loads. The analyses was computed with the finite element software Abaqus.

This thesis is part of Winfoor's project Triblade, that has the ambition to evolve the wind blade industry by modify the shape of a horizontal-axis wind turbine blade. The results and conclusions from this thesis are one of many things that has to be taken into account when the final design is developed.

1.3 Limitations

The following limitations apply:

- Linear elastic isotropic material properties are assumed
- The thickness of all sections will remain constant throughout the design
- No sandwich elements were used in FEM-model
- Colliding elements is not affecting each other
- The impulse loads created when the blades pass the tower will only be function of the wind speed, generated from a CFD analysis of a cylinder
- Gravity forces are not included

1.4 Outline of Thesis

1 Introduction	Background and purpose of the thesis.
2 Wind Turbine Blades	Short introduction of material and structural parts in wind turbines.
3 Theory	Introducing the theory for the analysis.
4 Finite Element Method Model	Describes how the FE model was developed from a CAD file as well as how the load was generated and applied to the structure.
5 Designing Sections of Triblade	Presents how the final design was decided using parametric studies.
6 Dynamic Analysis	The results and conclusions from the eigenvalue problem, frequency response analysis and the transient dynamic response
7 Conclusions	Conclusions from the performed study.

2 Wind Turbine Blades

2.1 Fiber-reinforced Polymers

Fiber-reinforced polymer (FRP) is a composite material made of a polymer matrix reinforced with fibers, which is a material very commonly used in the construction of aircrafts and wind turbines. The two most common FRPs used are glass fiber reinforced polymers (GFRP), and carbon fiber reinforced polymers (CFRP). Both of these materials combines a high stiffness and a low density in comparison to other materials, as shown in Figure 2.1. FRP also has a good fatigue performance, which is beneficial since the stress in the material will be varying due to the dynamic load (Brøndsted, 2005).

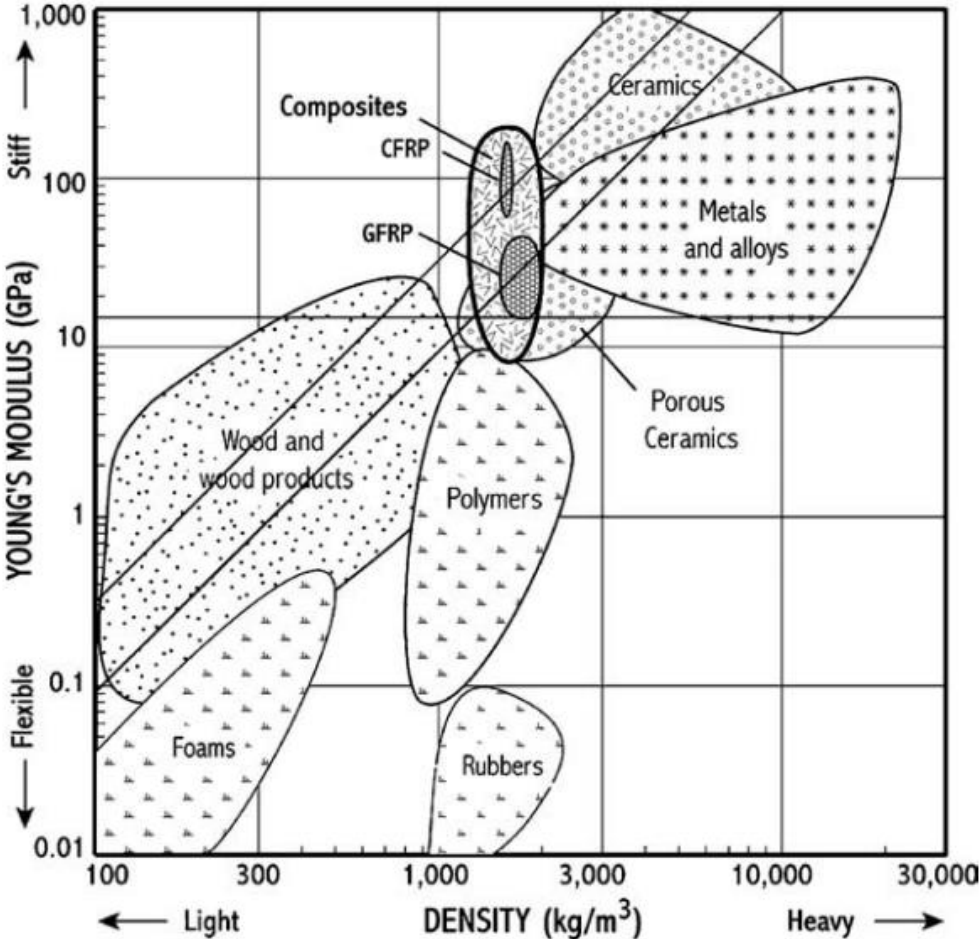


Figure 2.1: Diagram showing stiffness versus density for all materials (Brøndsted, 2005).

Glass fiber is the most widely fiber used in reinforced polymer, carbon fiber is stiffer and stronger but is also a lot more expensive. In Table 2.1 the materials properties for the fibers are shown.

Table 2.1 Material properties for fibers

<u>Fibers</u>			
Type	Young's Module E , GPa	Tensile strength σ_{fiber} , MPa	Density g/cm^3
Glass fiber	72	3500	2.54
Carbon fiber	350	4000	1.77

The material properties of reinforced polymers are depending on the amount of fibers compared to the amount the polymer used in the material. Therefore, it is possible to produce FRP with a wide range of stiffness. In Table 2.2 the material properties that will be used in this thesis are shown (Brøndsted, 2005).

Table 2.2 Material Properties for fiber reinforced polymers

<u>Composites</u>			
Composite	Young's Module E , GPa	Tensile strength $\sigma_{composite}$, MPa	Density g/cm^3
GFRP	38	1800	1.87
CFRP	176	2050	1.49

2.2 Wind Turbine Blade Design

The most basic structural concept of a wind turbine blade is a single load-carrying beam covered by a shell panel. The purpose of the shell is to define the shape of the airfoil and retaining the aerodynamic shape that creates the lift force. The forces are transmitted to blade support as a cantilever beam that is created from the structural core of the blade, spar cap and shear web (Bortolotti, 2012).

2.2.1 Structural Parts

The following terms are often used when studying the structural blade design.

- Airfoil – defines the shape of the cross section of the blade. It can be divided into a suction side and a pressure side.
- Chord line – represent the shortest line between nose and tail of the airfoil
- The span – is the length from the tip to the base of the blade
- Spar cap – the flanges of the load carrying cantilever beam
- Shear web – connects the two spars creating the load carrying beam
- Shell panel – defines the shape of the airfoil

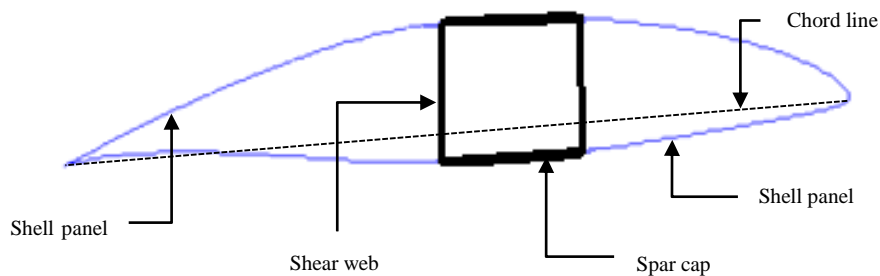


Figure 2.2: Structural parts for airfoil section

In this thesis the blade is assumed to be constructed using the following structural parts:

The load-carrying beam is built up by two spar caps and two stiffeners, often called shear webs, connecting the two spar caps. The spar caps are carrying the most normal forces and the webs are carrying the shear force. The spar caps are the heaviest loaded part of the structure and are therefore thicker and are often dominated by unidirectional (UD) fibers. The webs are usually made by sandwiching materials with composite skins and a core made from polyvinyl chloride (PVC) or a similar connector (Bortolotti, 2012). The aerodynamic shell panel is usually made of sandwich panels designed to avoid buckling during the compression state. These sandwich panels are not employed in this thesis. Instead they are modeled as regular shells elements.

2.3 Triblade Geometric

A sketch of the Triblade is shown in Figure 2.3. The Triblade contains six plates that divides each blade into five sections. Each plate is connected to another plate with six truss bars. The three blades are then connected to the hub with a root connection. In this thesis the root connection will be ignored, instead the boundary conditions will be enforced onto the plate closest to the hub.

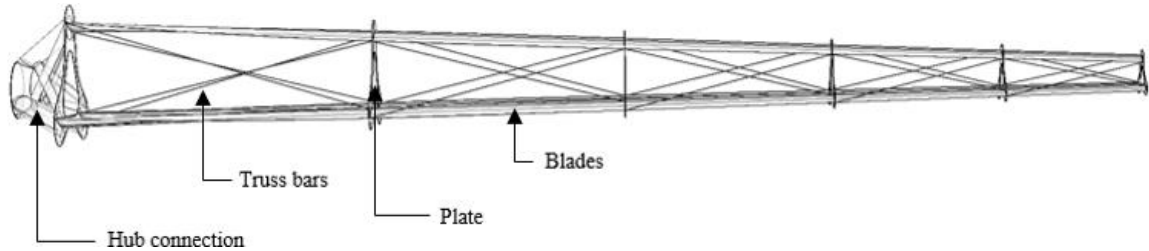


Figure 2.3: Design of the Triblade

2.3.1 Blades

The three blades are 60m long and are designed according to NREL's S831 Airfoil, see Figure 2.5. A blade is twisted in total 45.2° in order to optimize the lifting force. The chord varies linearly in length from 2m at the root connection to 0.75m at the tip.

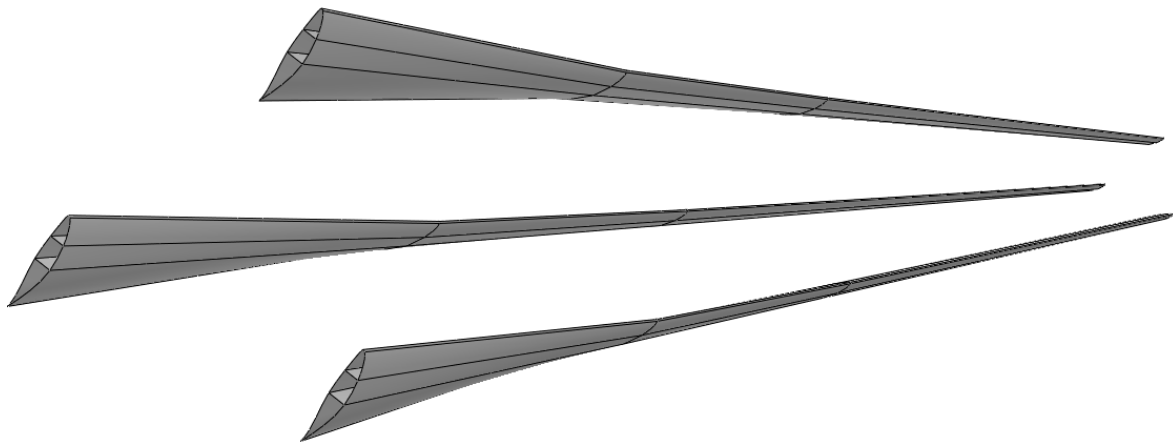


Figure 2.4: Blades of the Triblade

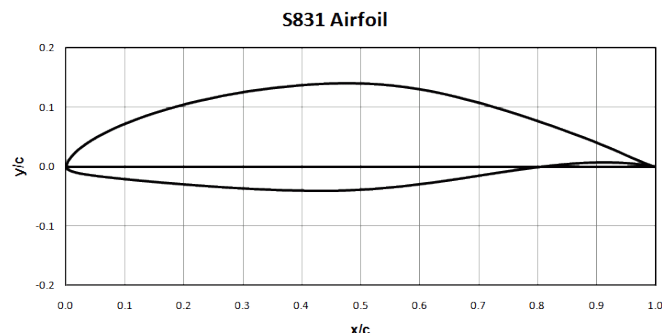


Figure 2.5: NREL's S831 airfoil graphic and coordinates

2.3.2 Plates

The six plates are fixing the positions of the blades. The plates are here assumed to be solid and have three airfoil shaped holes in which the blades can pass through.

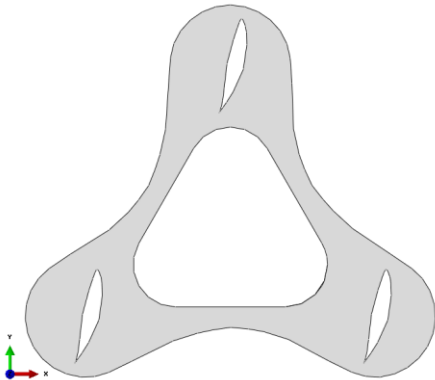


Figure 2.6: Geometric of plates

The six plates are creating five different sections. The largest section is closest to the hub, see Figure 2.7. The length of each section is listed in Table 2.3.

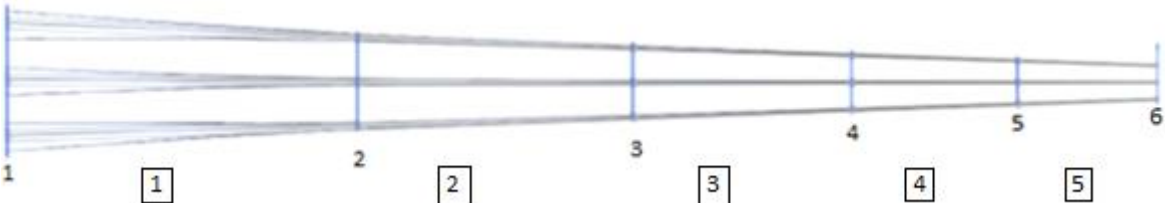


Figure 2.7: Plates placement and numbering of plates and sections

Table 2.3: Section length

Section 1	18.3m
Section 2	14.4m
Section 3	11.4m
Section 4	8.7m
Section 5	7.2m

2.3.3 Truss Bars

The truss bars are beams that are connected at the plates and creates the truss system that support the blade. Each truss bar is currently planned to have the shape of a neutral airfoil section in order to reduce forces from aerodynamic shape and sound emissions, see Figure 2.8.

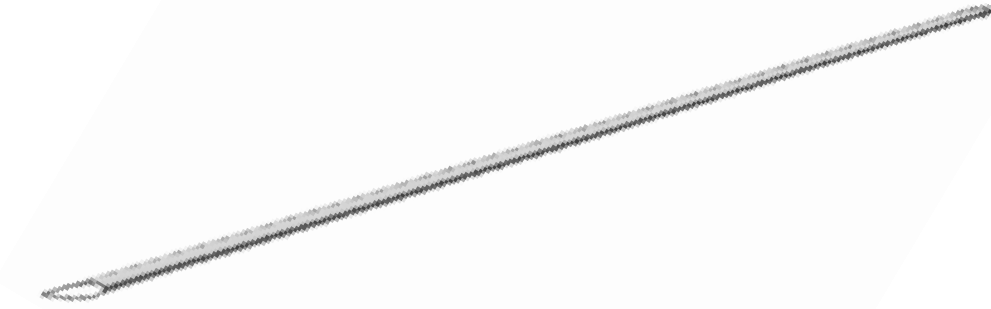


Figure 2.8: Truss bar in neutral airfoil

2.3.4 Truss System

In the original CAD model, each truss bar was connected to the plate either at the front edge or back edge of the blade, see Figure 2.9. This will generate bending moment if the forces in the two truss bars were not equal. A solution to avoid this was to connect all truss bars connected to the same point. In some cases, this was not possible since a truss bar then would have to cross through a blade. In those cases, the truss bars were instead connected to different points, see bottom left wing in Figure 2.10. The numbering of each truss bar within each section is presented in Figure 2.11.

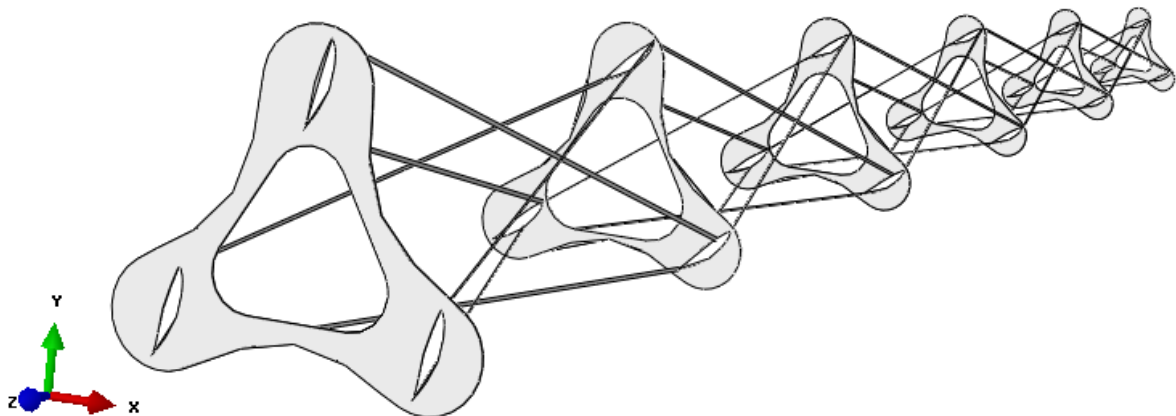


Figure 2.9: Original model

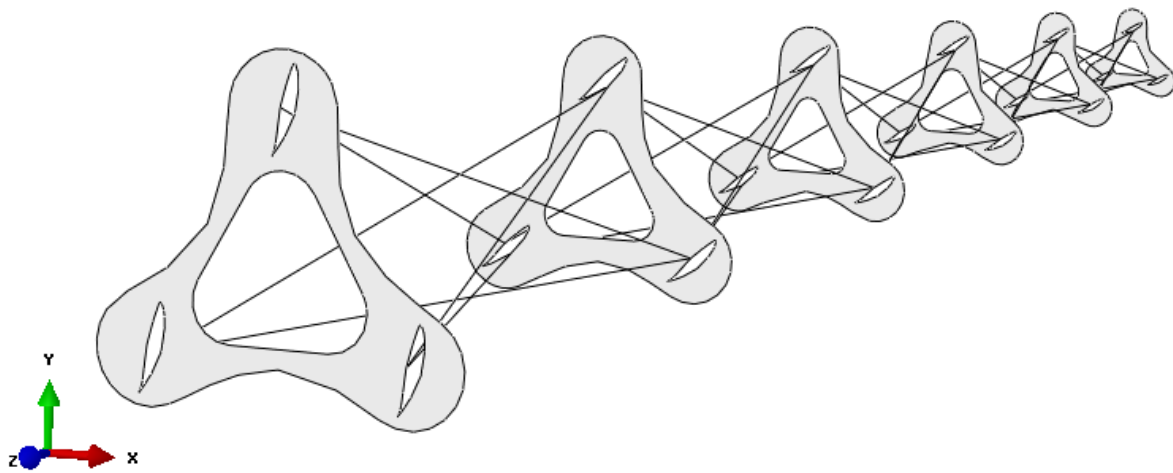


Figure 2.10: Updated model

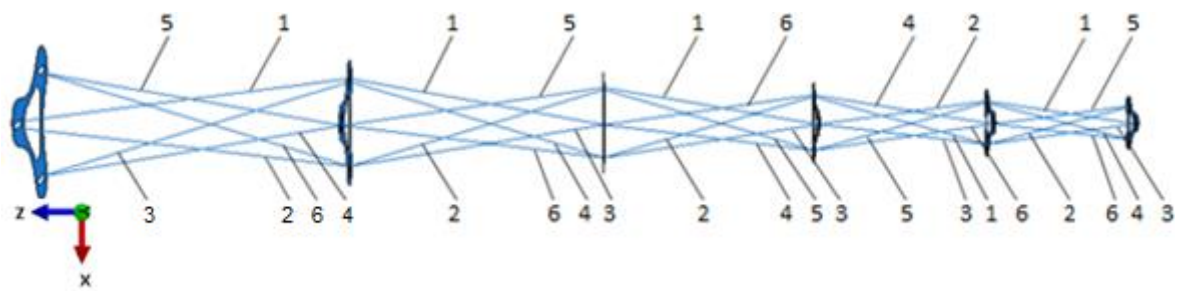


Figure 2.11: Numbering of truss bars

3 Theory

3.1 Finite Element Method

In engineering mechanics, the behavior may be formulated by partial differential equations, PDEs. If a PDE is too complicated to be solved by an analytical solution it is usually possible to solve it using a numerical approach often the finite element method (FEM). With the FEM the PDEs over a certain region are solved numerically in an approximated manner. The region may be one-, two- or three- dimensional. In the FEM each region is divided into smaller parts, so-called finite elements (FE), and an approximated displacement for each element is assumed. The collection of all elements inside a region is called a mesh (Ottosen 1992). The approximated solution is an interpolation over the element where the variable is assumed to be known at certain points. These points are often located on the boundary of each element and are called nodal points. The value at the nodal point is the unknowns of the problem. In this way a problem with an infinite amount of unknown has been reduced to a finite number of unknowns, these unknowns are called degrees of freedom, DOF.

The finite element formulation results in a linear system of equations,

$$\mathbf{K} \mathbf{u} = \mathbf{f} \quad 3.1$$

Where,

\mathbf{K} is the stiffness matrix

\mathbf{u} is the displacement vector

\mathbf{f} is the load vector.

3.1.1 Element Types

Two types of elements are used for the Triblade mesh, shell elements and beam elements (see Figure 3.1.)

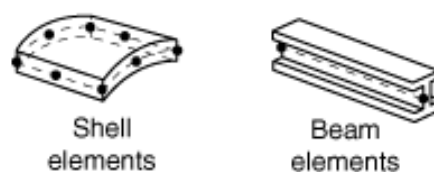


Figure 3.1: FEM elements

Depending on type, each element has different number of variables. For beam and shell elements, each node includes both translational and rotational DOFs.

3.1.1.1 3D Conventional Shell Elements

A 3D shell is as a surface element with a membrane and bending stiffness depending on the thickness of shell and the material properties. The stiffness in three directions enables a 3D shell element to transfer forces and moments in its plane as well as transverse to its plane.

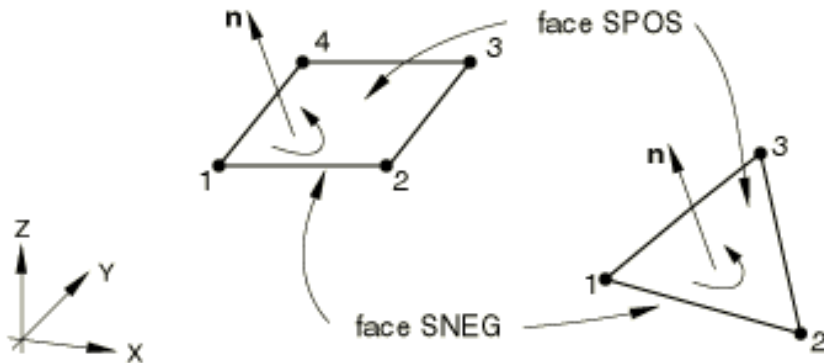


Figure 3.2: 4 node respectively 3 node 3D Conventional Shell Elements

A shell element has fewer DOFs as compared to a mesh with 3D solid elements and will therefore reduce the computational time for a solution. The shell type used in Abaqus is S3R and S4R, which are a 3-node respectively a 4-node doubly curved thin or thick shell, using reduced integration, hourglass control, and finite membrane strains.

3.1.1.2 Beam element

A beam geometry is based on a single line of two or three nodes for linear respectively quadratic geometry. Each node represents both translational and rotational DOFs to enable analyze a 3D behavior. The beam type used in Abaqus is B31, which is a 2-node linear beam in a 3D space.

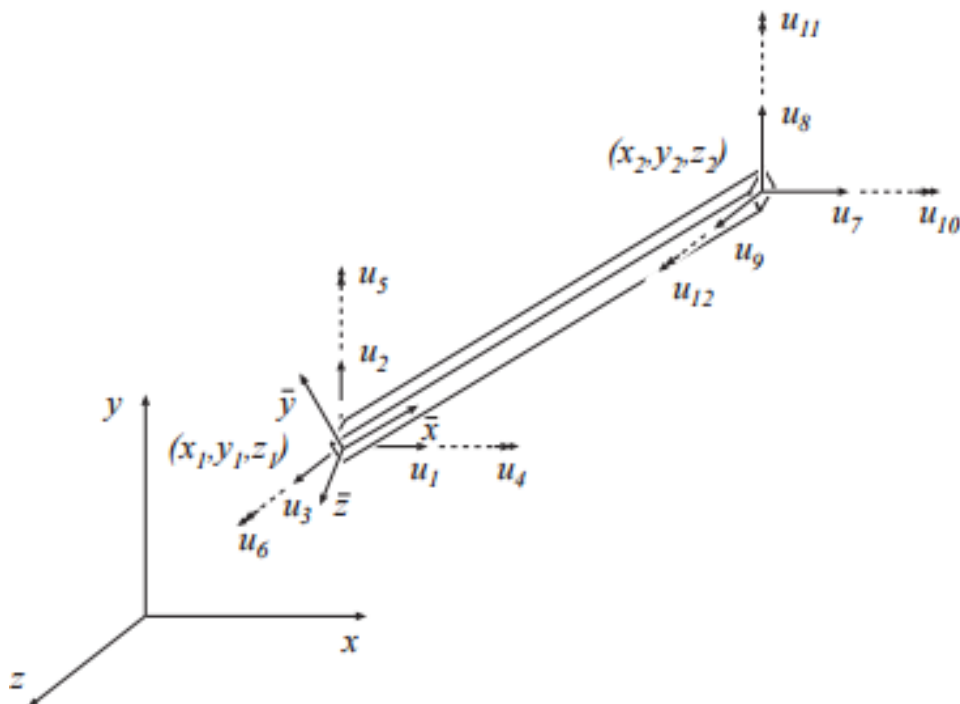


Figure 3.3: 3D beam element

3.2 Buckling

3.2.1 Geometric Nonlinear analysis

Nonlinearities can occur by large-displacement effect and material nonlinearity. Geometric nonlinearity arises when a structure undergoes large enough deformations to change the way the structure resists the load. There are many situations where a large deformation is coupled with plastic deformation, the following discussion will however assume the large deformation remains within the elastic range, this is also known as buckling (Zareh, 2008).

The major aspect of geometric nonlinearity is the coupling between the bending out-of-plane and the in-plane stiffness. The method to solve nonlinear buckling problem is to solve the equation $\mathbf{K}\mathbf{u} = \mathbf{f}$ where \mathbf{K} itself is a function of the displacement, written as $\mathbf{K}(\mathbf{u})$ (Cook, 2002).

Abaqus employs the Newton method to solve nonlinear problems. This approach subdivides the load into a series of increments to within each increment obtains equilibrium (Abaqus, 2015). If equilibrium is not achieved the calculation is recomputed by updating the stiffness matrix. Increments must be kept small enough to converge into a solution.

3.3 Structural Dynamics

3.3.1 Natural Vibration Frequencies and Modes

This section is introducing the eigenvalue problem, which gives the solution of the natural frequency modes of a certain system. For a multi degree of freedom system (MDOF) without damping the equation is given by (Chopra, 2009):

$$\mathbf{M} \ddot{\mathbf{u}} + \mathbf{K} \mathbf{u} = 0 \quad 3.2$$

Where \mathbf{M} is the mass matrix, \mathbf{C} is the damping matrix and \mathbf{K} is the stiffness matrix, $\ddot{\mathbf{u}}$ nodal acceleration, $\dot{\mathbf{u}}$ nodal velocity vector and \mathbf{u} nodal displacement.

The solution to deformation can be written in form:

$$\mathbf{u}(t) = \boldsymbol{\phi} e^{i\omega t} \quad 3.3$$

Where ω is the frequency. Substituting this form in Equation 3.1 gives the quadratic eigenvalue problem:

$$(\omega^2 \mathbf{M} + \mathbf{K}) \boldsymbol{\phi} = 0 \quad 3.4$$

Where the eigenvalue, ω , and the eigenvectors, $\boldsymbol{\phi}$, represents the natural modes.

The eigenvalue problem can be solved by taking the determinate of Equation 3.4

$$\det(-\omega^2 [\mathbf{M}] + [\mathbf{K}]) = 0 \quad 3.5$$

Solving this equation result in eigenfrequencice, ω_i that will be used in equation 3.3 to obtain the eigenvectors φ_i

$$\varphi_i = [\varphi_1, \varphi_2 \dots \varphi_n] \quad 3.6$$

This matrix is also called mode shape matrix since it carries information of the deformation shape, called mode shape, for each natural frequency, $\omega = [\omega_1, \omega_2, \dots, \omega_n]$. The mode shape visualizes the structures movement when excited by a certain frequency, ω_n .

Bending mode

A Triblade can be viewed as a cantilever beam, the shape of the first to fourth natural vibration mode expected in the Triblade are shown in Figure 3.4 (Chopra 2009).

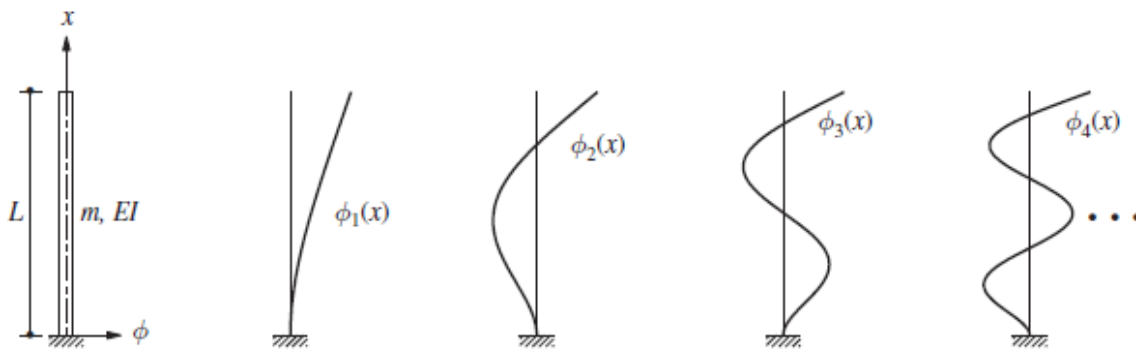


Figure 3.4: First to four natural bending modes of a cantilever beam (Chopra, 2009)

The truss bars in the Triblade on the other hand can be viewed as simply supported beams, the shape of the first to third natural bending mode that is expected for the truss bars are shown in Figure 3.5

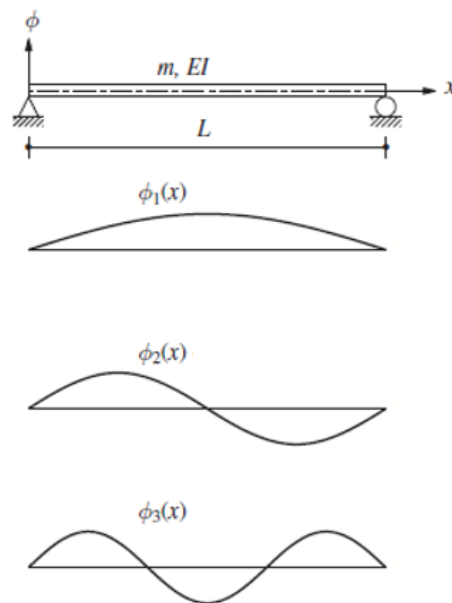


Figure 3.5: First to three natural vibration modes for a simply supported beam (Chopra, 2009)

3.3.2 Full Transient Dynamic Response

Transient dynamic analysis determines the dynamic response of a structure subjected to a time-dependent load. To compute the response in time, the equation of motion must be solved for the structure in time. The equation of motion for the transient dynamic response is:

$$\mathbf{M} \ddot{\mathbf{u}} + \mathbf{C} \dot{\mathbf{u}} + \mathbf{K} \mathbf{u} = \mathbf{f}(t) \quad 3.7$$

At any given time, t , this can be seen as a set of static equilibrium equations. Abaqus uses implicit time integration to solve the dynamic response of the structure. Where \mathbf{C} is the damping matrix.

3.3.3 Frequency Response Analysis

The method used to compute the structural response to steady-state (SS) oscillatory excitation is called frequency response analysis. In this analysis the excited response is defined in the frequency domain instead of in the time domain. All forces applied are known at each forcing frequencies and forces can be applied both as loads or displacements. In this thesis, a frequency analysis will be computed using a load that has been generated from a wind speed of 15m/s. This load is used for all frequencies.

Oscillatory loading is a sinusoidal and is in its simplest case defined as amplitude at certain frequencies. The steady-state response has the same frequency as the loading. The response can, due to damping be phase shifted. This leads to the peak response that might not occur at the same time as the peak load (Abaqus, 2015).

The computed response optioned includes displacements, velocities and acceleration for all nodes as well as stresses and forced for all elements in the model. The response is calculated as real vector, u_r and imaginary, u_i .

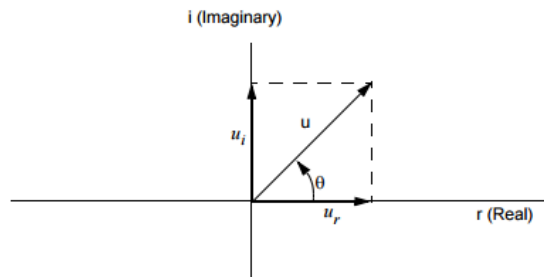


Figure 3.6: Real vector, u_r and imaginary, u_i .

Where the magnitude is:

$$u = \sqrt{u_r^2 + u_i^2} \quad 3.8$$

Phase angle is:

$$\tan^{-1} \left(\frac{u_i}{u_r} \right) \quad 3.9$$

There are two different methods used for computing the frequency response analysis. The direct method and the modal method. This thesis only adopts the direct method. In this method the equations of motion are solved from an oscillatory loading with varying frequencies.

The response is computed by solving the following matrix equation:

$$\mathbf{M} \ddot{\mathbf{u}}(t) + \mathbf{C} \dot{\mathbf{u}}(t) + \mathbf{K} \mathbf{u}(t) = \mathbf{P}(\omega) e^{i\omega t} \quad 3.10$$

The load is introduced as a complex vector. The harmonic motion response will also be complex and the solution is having the form:

$$\mathbf{u}(t) = \mathbf{u}(\omega) e^{i\omega t} \quad 3.11$$

Where $\mathbf{u}(\omega)$ is a complex displacement response vector. The velocity and acceleration is the first and second derivatives of Equation 3.11:

$$\dot{\mathbf{u}}(t) = i \omega \mathbf{u}(\omega) e^{i\omega t} \quad 3.12$$

$$\ddot{\mathbf{u}}(t) = -\omega^2 \mathbf{u}(\omega) e^{i\omega t} \quad 3.13$$

These expressions are inserted in Equation 3.16 giving the equation of motion expresses in the frequency domain:

$$(-\omega^2 \mathbf{M} + i \omega \mathbf{C} + \mathbf{K}) \mathbf{u}(\omega) = \mathbf{P}(\omega) \quad 3.14$$

3.3.4 Damping in Structures

It is hard to determine the damping matrix just based on the structural parts, member sizes, and the materials used. Therefore, damping is in general specified by numerical modal damping ratios. Damping ratios are used for analysis of linear systems with classical damping and is based from experimental data (Chopra 1995). A typical value for the damping ratio for a traditional wind turbine blade is 2% (Devriendt 2015). This value was adopted for the Triblade.

In classical damping is applying the damping mechanism distributed throughout the structure by making it mass- and stiffness-proportional damping. Using Rayleigh damping the damping matrix can be expressed as (Chopra 1995):

$$\mathbf{C} = \alpha \mathbf{K} + \beta \mathbf{M} \quad 3.15$$

Where α and β are the Rayleigh damping coefficients. Rayleigh damping follows the following equation:

$$\zeta = \frac{\alpha}{2 \cdot \omega_n} + \frac{\beta \cdot \omega_n}{2} \quad 3.16$$

This produces a curve where ζ is the damping ratio as a function of the natural frequency ω_n . The coefficients α and β can be determined from specified damping ratios ζ_i and ζ_j , i and j represent i th and j th mode. Expressing the two modes and assuming the damping ratios to be equal for both modes gives the following equation system.

$$\frac{1}{2} \begin{bmatrix} 1/\omega_i & \omega_i \\ 1/\omega_j & \omega_j \end{bmatrix} \begin{bmatrix} \alpha \\ \beta \end{bmatrix} = \begin{bmatrix} \zeta_i \\ \zeta_j \end{bmatrix} \quad 3.17$$

If both natural frequencies have the same damping ratio the Rayleigh damping coefficient can be calculated with:

$$\alpha = \zeta \frac{2\omega_i\omega_j}{\omega_i + \omega_j} \quad 3.18$$

$$\beta = \zeta \frac{2}{\omega_i + \omega_j} \quad 3.19$$

Using Equation 3.16 the damping ratios can be calculated over all frequencies (see Figure 3.7).

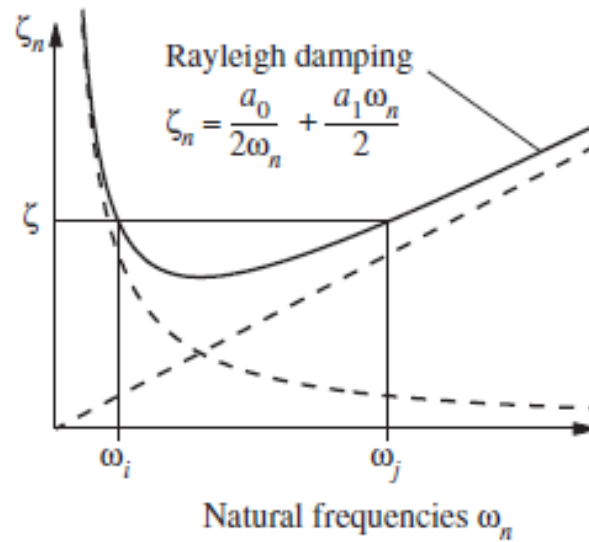


Figure 3.7: Variation of modal damping ratios with natural frequency using Rayleigh damping

4 Finite Element Method Model

4.1 Introduction

A large amount of FEM software exists. For the analysis in this thesis Abaqus/CAE was used. Abaqus/CAE was used to create the finite element model, solve the analyses, monitor and diagnose jobs and evaluate the results.

Python scripts were created to easily change the input file in the Abaqus model to efficiently change various parameters in the model.

A substantial time and effort was spent in developing the finite element model of a Triblade in Abaqus. In this chapter, the process of developing the FE-model from a CAD file is described. The changes that were made to the model as well as the motivation for these changes are also discussed. The developed model is later used in the static and dynamic analysis that are presented in Chapter 5 and Chapter 6.

Since a part of this thesis was to determine the section dimensions of each part it was important to create a model where changing the dimension of any section would not require a regeneration of the mesh. To fulfill this criterion, the blades, as well as the plates were modeled using shell elements with assigned thickness and the truss bars with beam elements with assigned cross-section.

4.2 Mesh and Simplifications

4.2.1 Plates

The plate was meshed by using Abaqus default Quad-dominated mesh generation scheme. This will primarily create 4-node elements and if necessary 3-node elements.

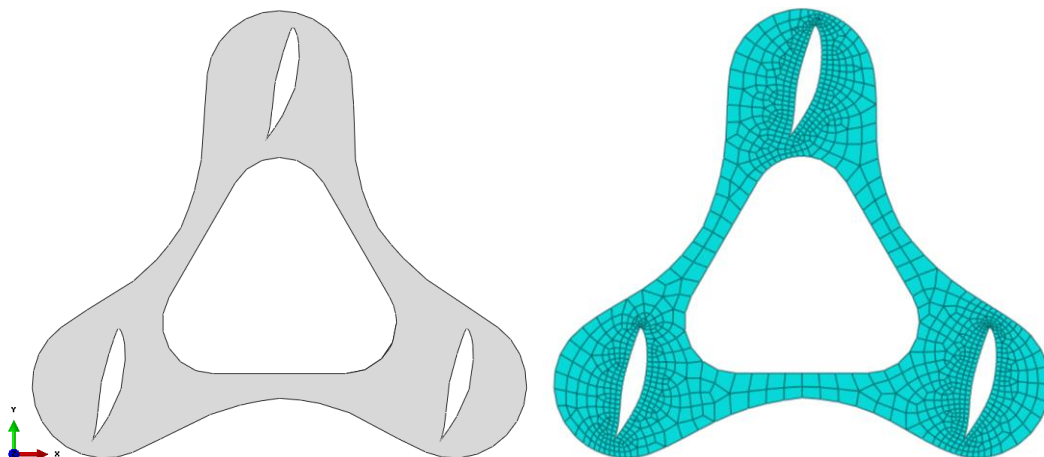


Figure 4.1: Mesh of plate

4.2.2 Truss Bars

The truss bars that are shaped as neutral airfoils modeled with beam elements with the section properties of a rectangular beam profile. By modeling the truss bars as beams enables easy changes of the dimensions of truss bars in the model. In order to have approximately the same stiffness as an airfoil is a rectangular with a cross section where $a \gg b$ is used, see Figure 4.2.

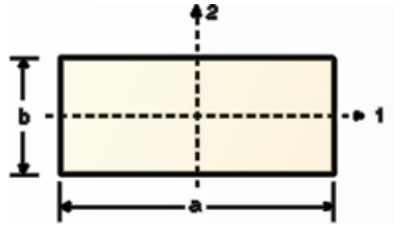


Figure 4.2 Cross section of beam

4.2.3 Blades

The blades in the Triblade were divided into three different sections: spar cap, shear web and shell panel as was mentioned in Chapter 2.1. All sections meshed with 4-node shell elements, see Figure 3.2.

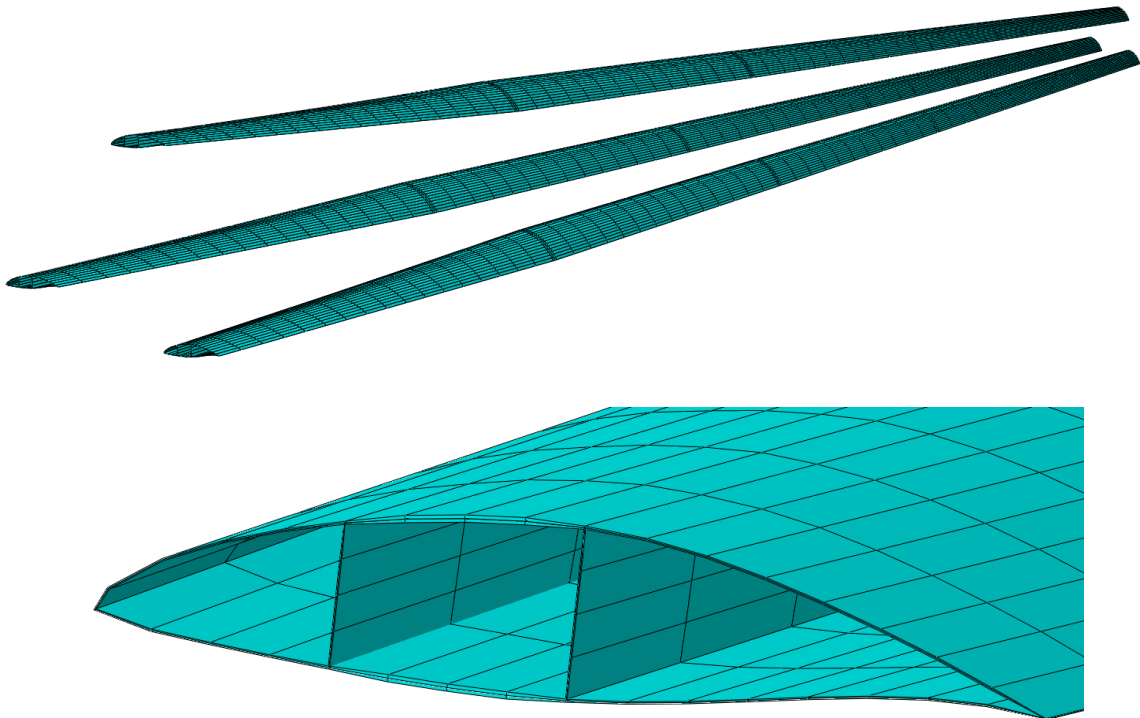


Figure 4.3: Mesh of blade

4.2.3.1 Interaction

A tie constrain was chosen between the plate, blade and truss bar. This means that the nodes in the contact between the parts has the same displacement and rotation.

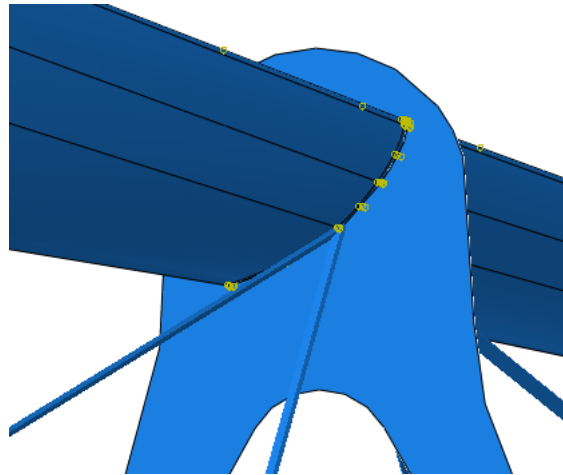


Figure 4.4: Tied interaction between plate, truss bar and blade

4.3 Material and Cross-Sections Properties

As mentioned in Chapter 2.1 two different materials was used in the model, the properties of these are shown can be seen in Table 4.1.

Table 4.1: Material properties of GFRP and CFRP

FRP			
Type	Stiffness E, GPa	Tensile strength σ, MPa	Density ρ, g/cm³
GFRP	38	1800	1.87
CFRP	176	2050	1.49

The material type assigned to each part is shown in Table 4.2.

Table 4.2: Material and section dimensions

Part	Material	Shell thickness (m)	Cross-section
Spar cap	CFRP	0.015	n/a
Shear web	CFRP	0.004	n/a
Shell panel	GFRP	0.005	n/a
Truss bar	CFRP	n/a	0.1 x 0.03

4.4 Boundary Condition

As mentioned in a previous chapter the root connection was in this model ignored. Instead the whole first plate was fixed, meaning that the displacement for all node of plate 1 was set to zero. To easily generate the total reaction forces where all nodes of this plate tied to a single node located at the center of the plate (see Figure 4.5) by use of infinitely stiff beams. This node was fixed in both rotation and displacement making all nodes on the plate fixed as well.

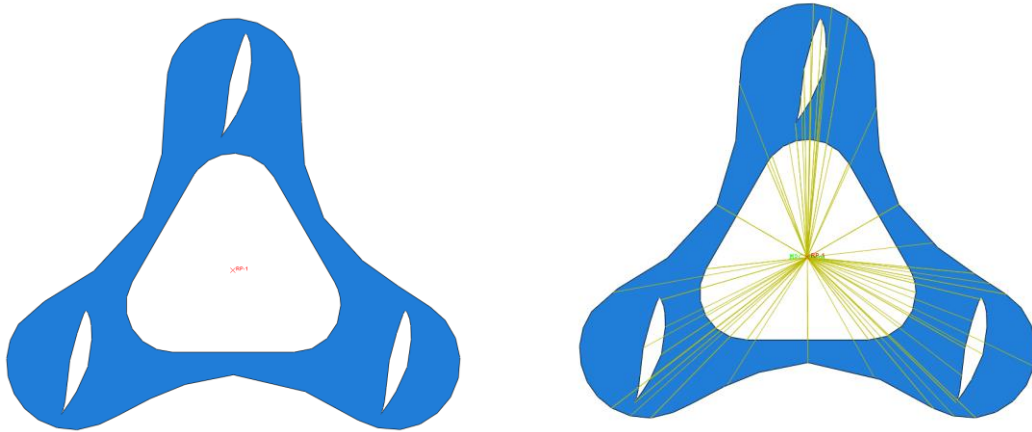


Figure 4.5: Boundary condition using infinitely stiff beams

4.5 Static Pressure Load

Wind turbines are one of the industrial structures that undergo most intense load during its life time (Söker, 2013). By being fully exposed to nature's forces and depending on the deployment of the site it also has to withstand both winds of various characteristics events like extreme heat or cold, solar radiation and erosion. They have to operate or must at least survive during any extreme condition that they may be exposed to. These design requirements are specified in a number of guidelines such as the IEC 61400-series (International Electrotechnical Commission). In IEC a number of design load cases listed, one of these are power production using a normal turbulence model and partial safety factors (IEC 61400-1, 1999). The partial safety factor is $\gamma = 1,35$. This safty factor, was multiplied with the pressure load from the wind load. The wind load was computed from a computational fluid dynamic (CFD) analysis that were computed in another thesis by Farah Salem, 2015. In the CFD analysis were the pressure distribution calculated around the airfoil by simulation the airflow around the airfoil.

For the CFD analysis the axial wind velocity was set to 15 m/s and it was assumed to be constant along the blade. Each blade section is also exposed to a tangential velocity caused by the rotation. The tangential velocity is perpendicular to the wind velocity.

The tangential velocity is varying linearly along the length of the blade, r , and is depending on the angular frequency, ω by:

$$v_r = r \cdot \omega \quad 4.1$$

The resultant wind velocity can be calculated as:

$$v_{eff} = \sqrt{v_r^2 + v_w^2} \quad 4.2$$

The angle between the v_{eff} and the chord line is called angle of attack, α . The lift and drag forces in Figure 4.7 are functions of v_{eff} and α .

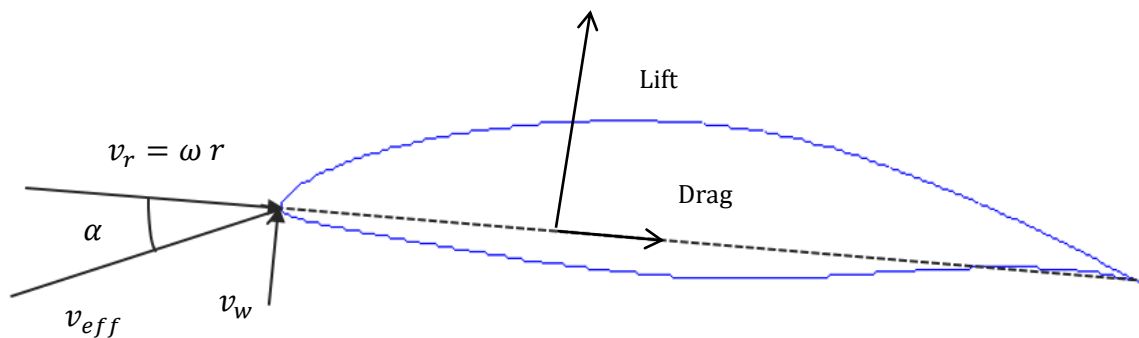


Figure 4.6: Wind velocity vectors

The Triblade has a design criterion that the tip speed is maximum six times the wind speed. This will generate a tip speed of 90m/s for a wind velocity of 15m/s.

4.5.1 Pressure Distribution over the Wing Profile

The lift force and drag force was in the FE-model applied as pressure distribution over the airfoil that was calculated in the CFD analysis. The CFD analysis was performed at three different locations along the Triblade, at the start of the blade ($r = 0m$), at the middle of the blade ($r = 30m$) and at the tip of the blade ($r = 60m$). The effective wind speed, V_{eff} , at these locations are 15 m/s, 47 m/s and 96 m/s, respectively.

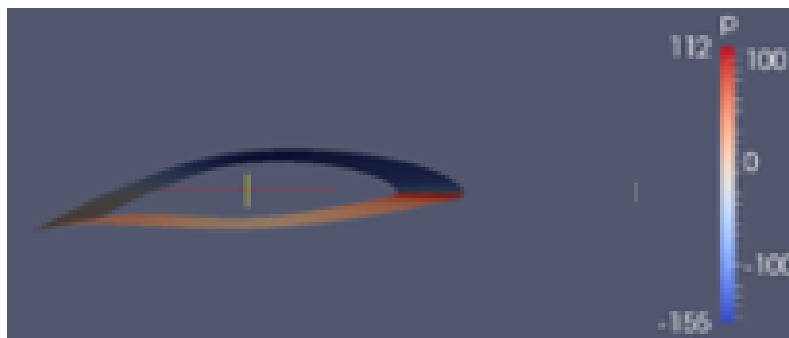


Figure 4.7: Pressure distribution around the airfoil for $v_{res} = 15$ m/s

To use the pressure data from the CFD in the FEM analysis it was necessary to find equations of the pressure distribution over the wing profile. This was determined as follows:

- The coordinates of the wing profile were normalized into a wing profile with a chord of 1m.

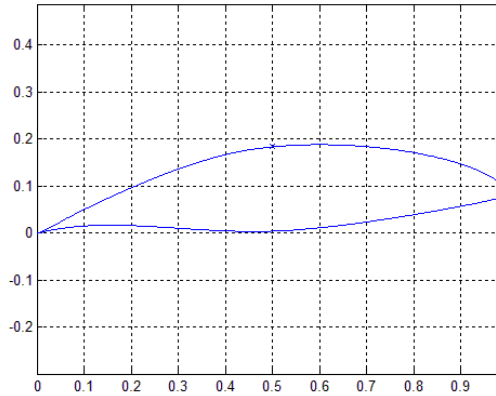


Figure 4.8: Airfoil profile with a chord of 1m

- The data was separated into two parts; one for the wing profiles upper surface, also called suction side, and one for the lower side, also called pressure side.
- The data for each pressure distribution is normalized by its respective absolute maxima comparison is shown in Figure 4.9.
- A sixth degree polynomial is then fitted to the normed curves to generate an equation of how the pressure is varying over the x-coordinate over the airfoil (see dashed line in Figure 4.9). Note that a negative pressure on the upper side of the airfoil results into a lifting force on the blade and positive pressure at the lower side of the airfoil also results into a lifting force on the blade.

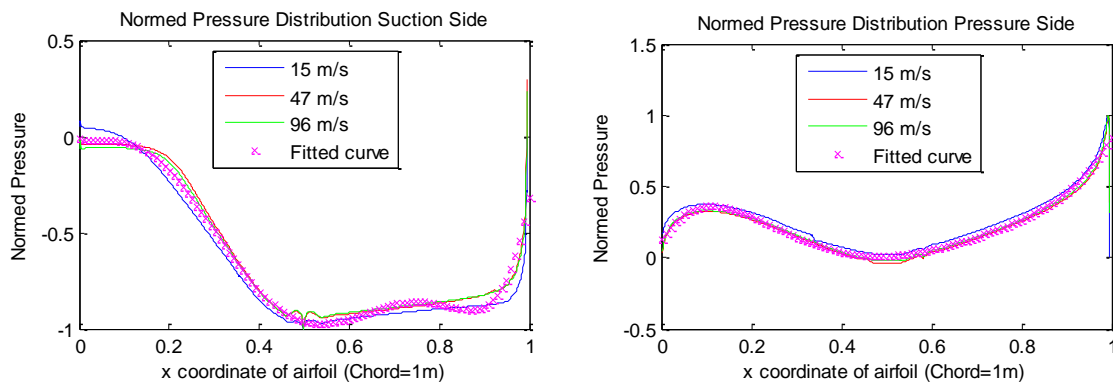


Figure 4.9: Normed pressure distribution over airfoil

The equation of the pressure variation along x-axis at the suction side for a chord of 1m is:

$$p_{normed} = 153.12x^6 - 414.683x^5 + 400.01x^4 - 155.98x^3 + 17.984x^2 - 0.76029x - 0.01231 \quad 4.3$$

The equation of the pressure variation along x-axis at the pressure side for a chorda of 1m is:

$$p_{normed} = 25.988x^5 - 71.671x^4 + 74.237x^3 - 32.786x^2 + 4.9443x + 0.12611 \quad 4.4$$

These equations are only applicable to a chorda on 1 meter. The Triblades chorda length variates from 2m to 0.5m. When these equations are adopted into the FE-model are a scaling equation required. This scaling equation is further explained in Chapter 4.5.2.

- The three maximum from the CFD analysis was then used for creating a function for the pressure along z-direction (direction of the blade). The pressure distribution in the z-direction was calculated by using the absolute maximum for the three CFD analysis. A second degree equation was then fitted to the data.

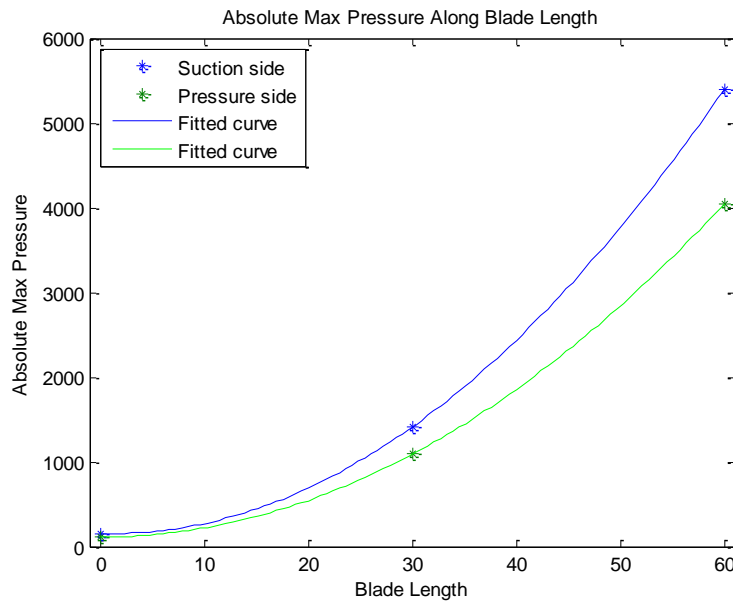


Figure 4.10: Pressure magnitudes along length of blade

The equation of the pressure variation along z-axis at the suction side for a chorda of 1m is:

$$p_{magnitude} = 1.5176z^2 - 3.710z + 155.43 \quad 4.5$$

The equation of the pressure variation along z at the pressure side for a chorda of 1m is:

$$p_{magnitude} = 1.0991z^2 - 0.43467z + 122.26 \quad 4.6$$

4.5.2 Application of Load to Model

To implement equations 4.3 – 4.6 in the FE-model, the blades were divided into five sections each with a local coordinate system placed at the middle of each section. The load was assumed constant along the length of each section but to vary over the airfoil profile. The following chapter is describing how to create a load equation that applies a pressure force constant along the length of each section but to vary over the airfoil profile.

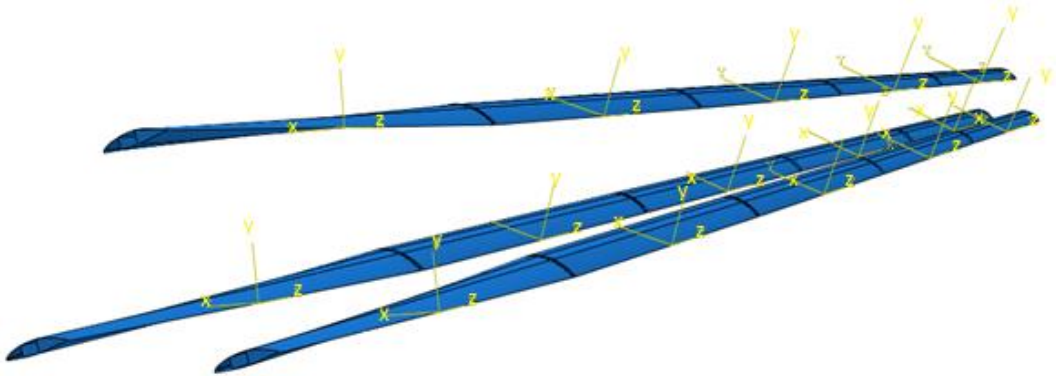


Figure 4.11: Local coordinate systems along length of blade

4.5.2.1 Chord length

In each coordinate system the chord length is decreasing linearly from start to end. The pressure distribution calculated in CFD was only based on the x-axis in Figure 4.11. To implement the load with the right pressure distribution over the whole blade must the load be scale along the length of the blade.

As the chord length are decreasing linearly with $k = 0.0208m/m$. The load is modified by adding a factor based on the z-coordinate and the mean chord length of each local coordinate system.

$$x' = x \frac{(1 + 0.0208 z)}{c_{mean}} \quad 4.7$$

Where x and z are the local coordinates in Figure 4.11, c_{mean} is the mean chord length of the section and x' are the variable between 0 and 1 used to calculate the normed pressure magnitude of load in equation 4.3 and 4.4. The mean chord length is listed in Table 4.4.

Table 4.3: Mean chord of each section

Section	Length of section (m)	Mean chord length, c_{mean}
1	17.1	1.82
2	14.05	1.50
3	11.55	1.23
4	9.5	1.01
5	7.8	0.833

4.5.2.2 Rotation

Additionally, each blade is rotated around the trailing edges along the z-axis in each coordinate system as shown in **Figure 4.12**.

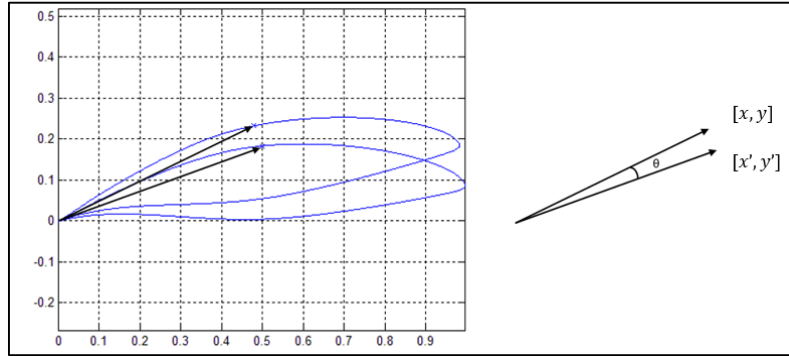


Figure 4.12: Airfoil profile at center of coordinate system compared to airfoil profile at the end of section

Each section is rotated a certain amount of radians per meter along the blade.

The not rotated coordinates (x' and y') are calculated from the rotated coordinates with the rotation matrix, see Equation 4.7.

$$\begin{bmatrix} x' \\ y' \end{bmatrix} = \begin{bmatrix} \cos(\theta) & -\sin(\theta) \\ \sin(\theta) & \cos(\theta) \end{bmatrix} \begin{bmatrix} x \\ y \end{bmatrix} \quad 4.7$$

And,

$$\theta = \varphi \cdot z \quad 4.8$$

Where θ is the rotation angle of each airfoil profile that are a function of the rotations constant, φ , given in *radians/m* for each section. The rotation constant is multiplied by z-coordinate to give the rotation of each profile in each section. Since the pressure distribution function is only depending on the x-coordinate can Equation 4.7 be rewritten as:

$$x' = \cos(\theta) x - \sin(\theta) y \quad 4.9$$

The rotation constant (φ) for each section is shown in Table 4.3.

Table 4.4: Rotation constants for each section

Section	Length (m)	φ (radians/m)
1	17.1	0.0349706
2	14.05	0.0180686
3	11.55	0.0173793
4	9.5	0.0176142
5	7.8	0.0483078

By include both the factors from equation 4.7 and 4.10 the total transformation equation is created by:

$$x' = (\cos(\theta) x - \sin(\theta) y) x \frac{(1 + 0.0208 z)}{C_{mean}} \quad 4.11$$

4.5.2.3 Load function

Using both the pressure distribution function (Equation 4.3 and 4.4) together with the scale function Equation 4.11 the pressure function can be written as an equation system. The equation system calculates the pressure from the local coordinates. Where the pressure for each element are normed, $-1 \leq p_{normed} \leq 1$.

The normed pressure for the upper side of the airfoil profile can be calculated using the following equation system:

$$x' = (\cos(\theta) x - \sin(\theta) y) \frac{1 + 0.0208 z}{c_{mean}} \quad 4.12$$

$$p_{normed} = 153.12x'^6 - 414.683x'^5 + 400.01x'^4 - 155.98x'^3 + 17.984x'^2 - 0.76029x' - 0.01231$$

The normed pressure for the lower side of the airfoil profile can be calculated using the following equation system:

$$x' = (\cos(\theta) x - \sin(\theta) y) \frac{1 + 0.0208 z}{l_c} \quad 4.13$$

$$p_{normed} = 25.988x'^5 - 71.671x'^4 + 74.237x'^3 - 32.786x'^2 + 4.9443x' + 0.12611$$

The p_{normed} will multiplied with an amplitude for each section. The amplitude can be calculated from Equation 4.5 and 4.6. The z-value in this function, are the distance from plate 1 to center of each local coordinate system and is shown in Table 4.5.

Table 4.5: Pressure amplitude for each section

Section	Distance from plate 1 to center of coordinate system (m)	Upper side	Lower side
		$p_{magnitude}$ (Pa)	$p_{magnitude}$ (Pa)
1	8.550	234.7	188.9
2	24.13	949.2	741.5
3	36.93	2088	1595
4	47.45	3396	2566
5	56.10	4724	3547

Total load applied to the model is shown in Figure 4.13. In total is this force $F_{dim} = 375.309kN$. Note that in the visualization the force arrows are scaled for each section.

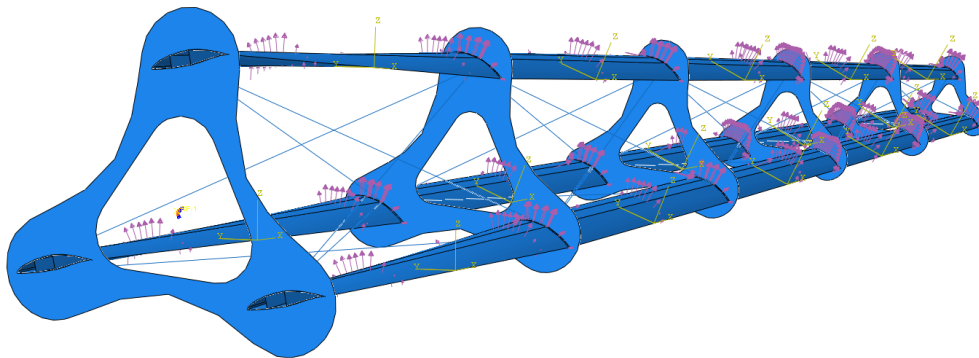


Figure 4.13: In the model 3x5 loads are applied to the blade

4.6 Dynamic load

A dynamic load was applied to compute the transient dynamic response of the structure. The load that was examined was from the blade-tower interaction. The dynamic load from the blade-tower interaction was approximated from models that has determined the velocity field in front of the tower. The following section described the method of how this velocity field was converted into an impulse load.

4.6.1 Undisturbed Tower-Flow

The simplest way to describe the interaction between the tower and the blade is by assuming that the flow around the tower is similar to the airflow around a two dimensional cylinder. A model of the flow around a cylinder has been computed in (Gómez, 2009). In this article the flow around a cylinder is modeled using the software AeroDyn. The velocity field calculated using this model is shown in Figure 4.14. The velocities are normalized with respect to the inlet velocity.

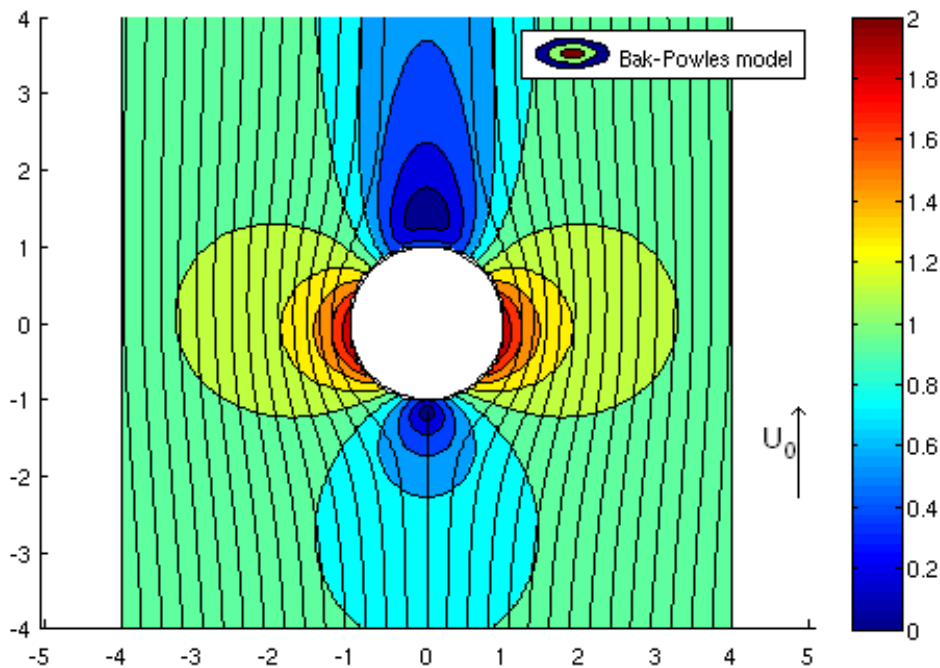


Figure 4.14 Velocity field as implemented in AeroDyn (Gómez, 2009).

For the interaction between the tower and the blade, the distribution of the wind velocity in front of the tower is governing the impulse load. The distribution of the axial and the tangential velocities in front of the tower is shown in Figure 4.15.

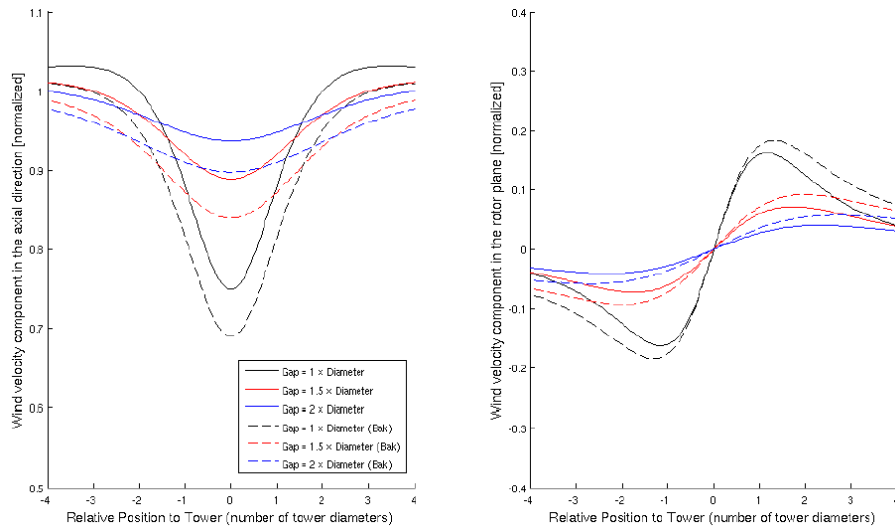


Figure 4.15: The axial and the tangential velocities in front of the tower (Gómez, 2009)

This figure shows the results from two different models at three different distance from the blade to the tower, here called gap. Gap is defined as the distance from the center of the towers to the rotation plane of the blades. In this thesis the selected gap was assumed to be the same for all the three blades in the Triblade, this is $Gap = 1 \times Diameter$, where the diameter is the diameter of the tower. The curve that describes the undisturbed tower-flow is assumed to be the black dashed curve in Figure 4.15.

The impulse will only be applied on the three wing sections closest to the tip since it is on the lower part of the tower where the two dimensional airflow is accurate.

For the case when an airfoil profile is approaching the tower passage, the operative wind velocity (due to the rotation of the wind turbine) is directed in the same direction as the tangential velocity from the velocity field. This leads to a higher total wind velocity and therefore an increased lifting force is acting on the blade.

When the blade has passed the tower the tangential wind velocity is directed in the opposite direction and the total wind velocity is reduced generating a decreased lifting force, see Figure 4.16. This will create a total impulse where the force is first increased and then decreased.

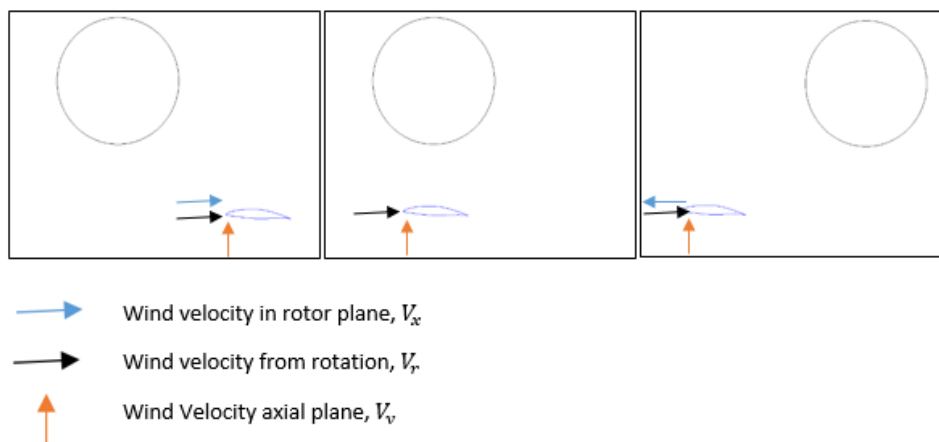


Figure 4.16: Illustration of the tower passage. In the left figure are the airfoil approaching in the tower passage. In the middle are the airfoil located in front of the tower. In right are the airfoil leaving the tower

With the notation in figure 4.16, the resultant wind velocity is calculated as:

$$V_{tot} = \sqrt{(V_x + V_r)^2 + V_y^2} \quad 4.14$$

4.6.2 Connection from Velocity to Force

The wind pressure was assumed to only be a function of the wind velocity, this function was generated from the data from the CFD analysis and is shown in Figure 4.17.

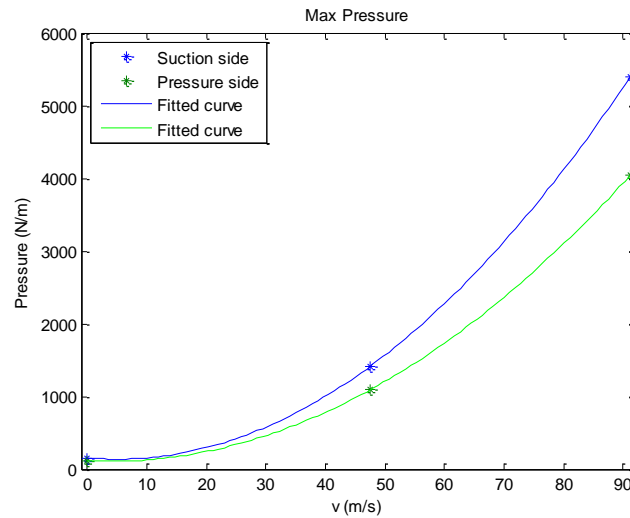


Figure 4.17: Pressure as a function of velocity

The angle of attack will also change from the optimal angle during the tower passage and thereby reducing the lifting force. This effect is however neglected.

4.6.3 Data for Impulse

The wind turbine is designed to utilize a tip speed ratio of 6 times the wind speed. The angular frequency is:

$$\omega = \frac{2\pi}{T} = \frac{ratio \cdot V_{wind}}{R} \quad 4.15$$

where, $R = 60m$, The blade length, $ratio$, is $\frac{V_{tip}}{V_{wind}} = 6$ and $V_{wind} = 15m/s$ Is the wind speed.

Three different impulses were created for the three outermost sections of the blade. The impulse has a duration time of 0.82 seconds and starts when the blades are not interacting with the tower. The different locations that was used for calculation the impulse is listed in Table 4.6. Here d is the distance to the tower and α the angle between the blade and the tower.

Table 4.6: Relation between distance to tower and time

	Distance, d (m)	α (rad)	Time, s
1	34.88	0.9503	0
2	15	1.318	0.2451
3	21.75	1.200	0.1663
4	10	1.403	0.3012
5	5	1.487	0.3580
6	0	1.571	0.4136
7	-5	1.654	0.4692
8	-10	1.738	0.5252
9	-15	1.823	0.5821
10	-21.75	1.942	0.6609
11	-34.88	2.191	0.8272

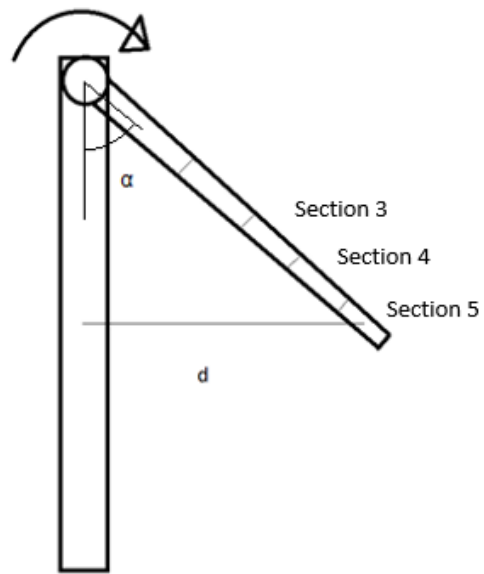


Figure 4.18: Geometry constants

With the data it is possible to create the impulse. The velocities together with the rotation velocity generates the total wind velocity. With the total wind velocity, the pressure is obtained by use of the results in Figure 4.17. The resulting pressure is presented in Figure 4.19.

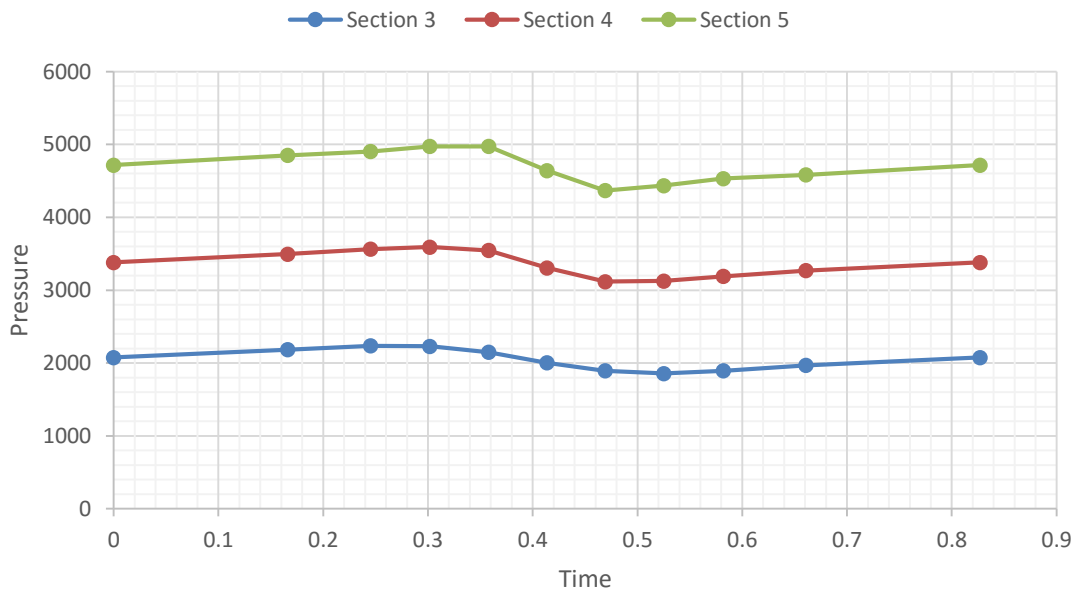


Figure 4.19: Pressure changes in time during tower passage

The impulse was in the finite element model applied as an amplifier to the static pressure load in equation 4.3:

$$P_{impulse}(t) = Amp(t) \cdot P_{static} \tag{4.16}$$

Two different impulse analyses were computed in this thesis. In the first analysis the structure was only loaded with the impulse load. In the second analysis the static load was applied before the impulse was added. Depending on if the structure was loaded by the static load first different impulses were used, these are shown in Figure 4.20 and Figure 4.21.

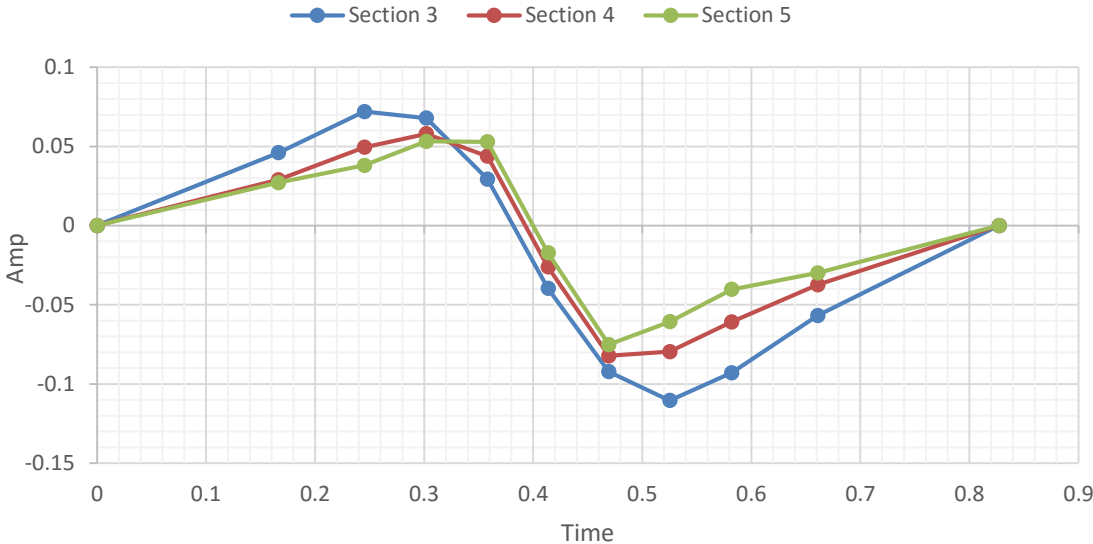


Figure 4.20: Amplitude in time added to create an impulse to an unloaded structure

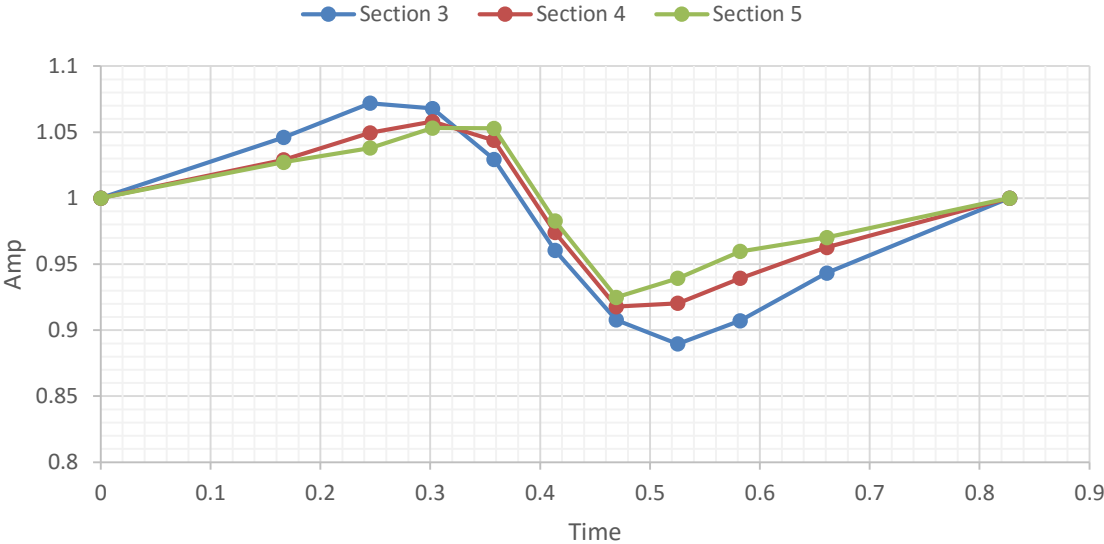


Figure 4.21: Amplitude in time added to create an impulse to an already loaded structure

4.6.4 Damping Coefficients

As mentioned in Chapter 3.3.4 the damping ratio was set to 2% of critical damping. The Rayleigh parameters were calculated for the frequency 2.15Hz and 8.0 Hz. The damping ratio for all frequencies was calculated using the Rayleigh damping equation (Equation 3.18 and 3.19) and is shown in Figure 4.22.

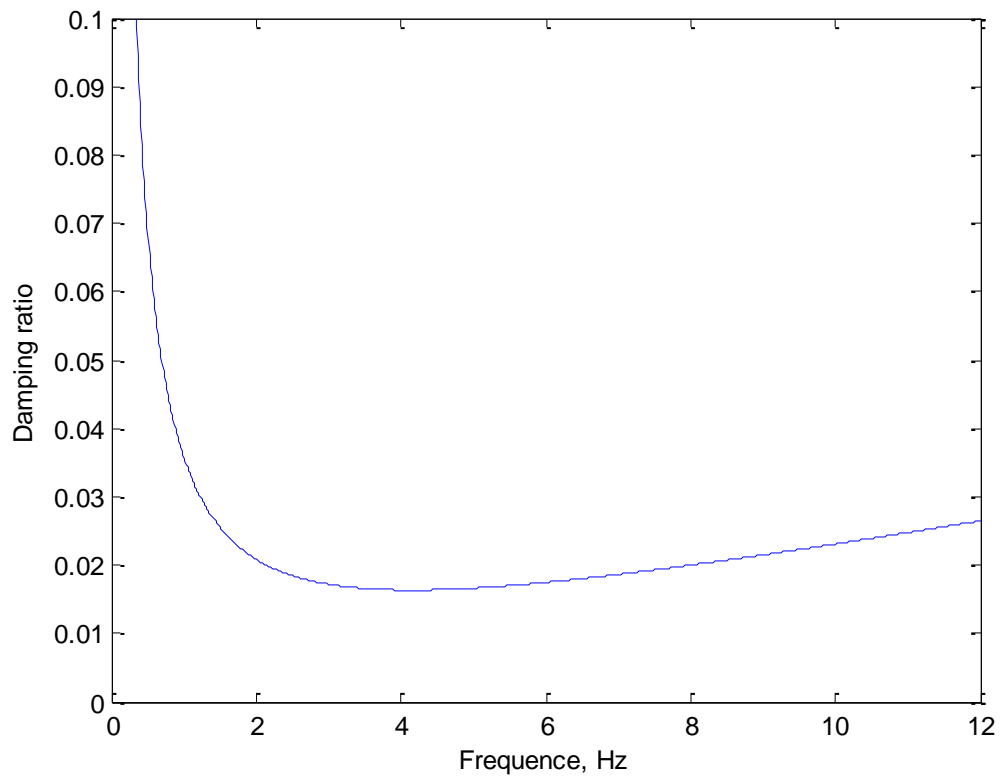


Figure 4.22: Damping ratio over frequencies

5 Designing Sections of Triblade

5.1 Chapter Abstract

The stability of the Triblade structure was first analyzed by computing its critical buckling loads. A common way to analyze this is in a linear buckling analysis. In a linear buckling analysis buckling problem the loads are calculated for which model stiffness matrix becomes singular. The eigenvalue analysis is however best used when estimating the critical buckling load of an ideal structure e.g. a column. When a structure is more detailed and it undergo large deformations before buckling it is more accurate to use a nonlinear analysis (Novoselac, 2012). This is the reason to why there is only made a nonlinear buckling analysis in this thesis.

Since the truss bars in the Triblade are long and slender they are very likely to buckle when a compression force is applied to the truss bar. When truss bars are buckled, the stiffness of that truss bar decreased to zero. This means that additional forces after the truss bars in compression are buckling have to be carried by the rest of the structure.

5.2 Objective

The main objective of the static analysis was to find a design proposal for the members of the Triblade structure that has higher loading capacity than the static pressure load generated by the CFD analysis described in Chapter 4.5. This model was then used in the dynamic analyzes. In the design proposal, each part of the structure was assigned a section thickness and a material.

5.3 Method

Two parametric studies were completed in order to find a design proposal for the Triblade. In the first parametric study the Young's modulus was varied for the different structural sections. This study was made to determine how much each part of the structure was contributing to the total stiffness of the structure and the result from this analyze was used to assign a material for each structural part. This analysis was made in the beginning of the project before the static pressure load in Chapter 4.5 was developed. In the parametric study the load was applied as a constant pressure on the pressure side of the blades throughout the length of the blade.

A different load was used in the second parameter study therefore the load capacity cannot be compared between the two analyses. In the second analysis the load was applied as a quadratic increasing load towards the tip. Therefore a higher moments were obtained in this analysis achieved in this analysis. Lower load capacity was then obtained for the second analysis although the structure was identical.

In the second parametric study different section dimensions were tested in order to find the final design of the Triblade that would give a buckling load higher than the dimension load, F_{dim} , calculated in the CFD analysis.

Large deformation analysis was used in all simulations. This step applies the increments until the structure becomes unstable, a buckling load is reached. Since the simulations are in load control, the solution will not converge after a maximum load is reached. The critical buckling load for each tested structure is thus found. In the parameter analysis the magnitude of the total force, F_{dim} , was increased compared to the load from the CFD analysis in order to always make sure that a maximum load was found.

5.4 Results and Analysis

5.4.1 Parametric Studies of Varying the Young's module

In the parametric analyses, five different structural sections are evaluated. These are plate, truss bar, shell panel, spar cap and web shear. Shell panel, spar cap and web shear are all different parts of a blade as shown in Figure 5.1. The results from the analysis are used to assign a material to each section.

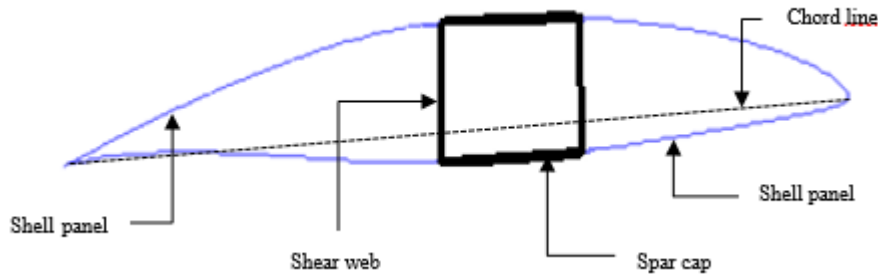


Figure 5.1: Structural sections

In this analysis all section dimensions were kept constant and they are listed in Table 5.1, only the Young's modulus for one part at a time is changed in each calculation.

The Young's modulus is varied between 20 GPa and 176 GPa since it is approximately the Young's modulus of GFRP and CFRP.

Table 5.1: Section dimension in model

Part	Section dimension (mm)
Plate thickness	30
Truss bar cross-section	80x80
Shell panel thickness	2
Spar cap thickness	10
Web thickness	10

5.4.1.1 Example of Buckling Mode

The most common buckling mode from the first parameter study were buckling of shell panel of the airfoil. An example of the buckling mode is show in Figure 5.2.

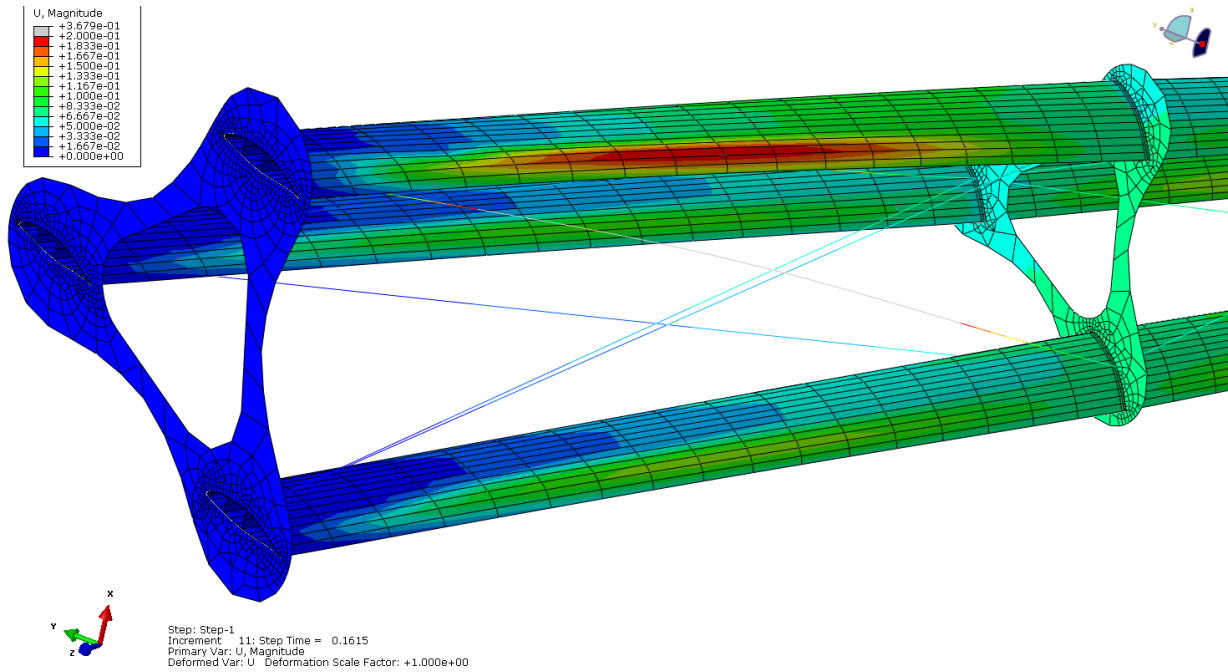


Figure 5.2: Buckling of shell panel in section 1

The material and section dimensions this calculation is shown in Table 5.2. The critical load capacity for the mode were $F_{crit} = 383 \text{ kN}$.

Table 5.2: Material and section dimetions

Part	Section dimension (mm)	Young's module (GPa)
Plate	30	38
Truss bar	80x80	176
Shell panel	2	30
Spar cap	10	176
Web	10	176

In Figure 5.3 it is shown that the load-displacement the curve for tip is linear but for the shell panel nonlinear. This indicates that it is the trailing shell panel that is causing the structure to become unstable.

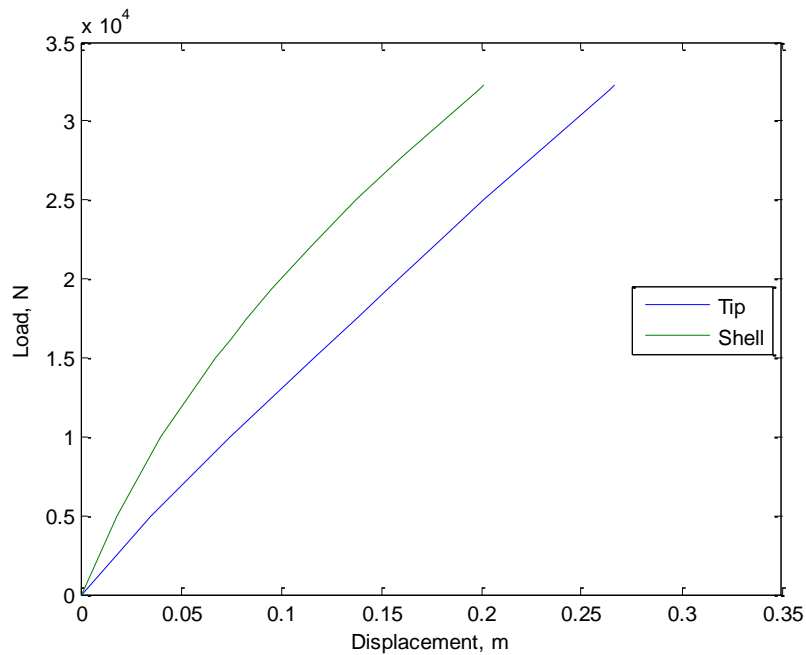


Figure 5.3: Load-displacement the curve for a node located on the buckling shell in section 1 and a node the tip of the wing

5.4.1.2 Shell Panel Stiffness

Changing of the Young’s modulus of the shell panels will change the stiffness of the Triblade. The stiffness of the structure is changed is evaluated by computing the buckling load for each setup.

The Young’s modulus was changes between 20 and 176 GPa in nine different setups. The Young’s modulus for the rest of the structure are shown in Table 5.3.

Table 5.3: Young’s module for each part of the structure

Part	Young’s module (GPa)
Shell panel	20-176
Plate	38
Truss bar	176
Spar cap	176
Shear web	176

The buckling load were calculated for the nine different values of the Young's modules. The buckling capacity for each setup are shown in Figure 5.4.

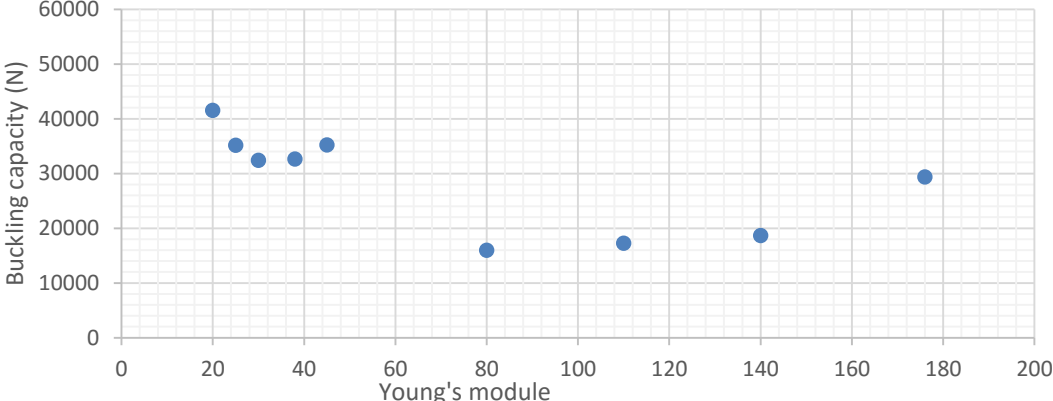


Figure 5.4: Buckling capacity vs. Young's module for shell element

5.4.1.3 Plate Stiffness

In similar way as for the shell panel where the influence of the plates contribution to the stiffness of the whole structure evaluated in this study. The Young's modulus was changes between 30 and 176 GPa for the plate section. The Young's modulus for the rest of the structure are shown in Table 5.4.

Table 5.4: Young's module for each part of the structure

Part	Young's module (GPa)
Shell panel	30
Plate	30-176
Truss bar	176
Spar Cap	176
Shear Web	176

The buckling load were calculated for six different values of the Young's modules. The buckling capacity for each setup results are shown in Figure 5.5.

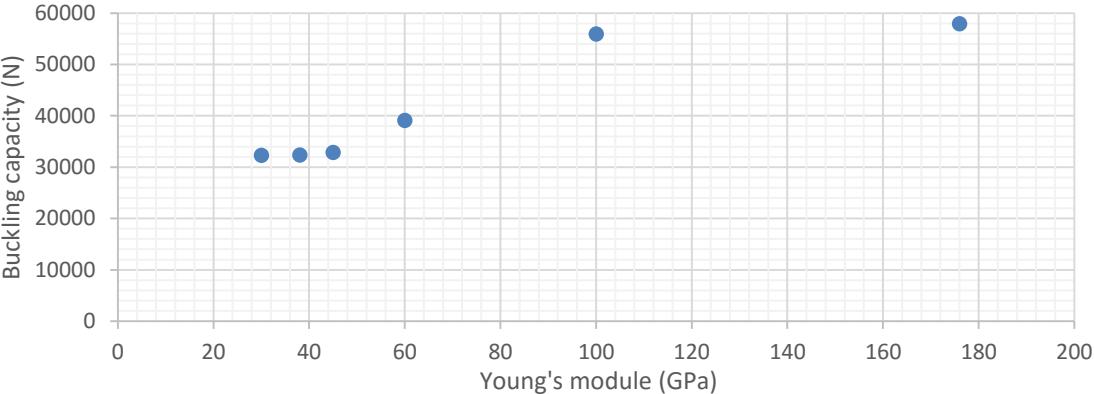


Figure 5.5: Buckling capacity vs. Young's module for plate element

5.4.1.4 Spar Cap Stiffness

The Young's modulus was changes between 40 and 176 GPa for the spar cap section. The Young's modulus for the rest of the structure are shown in Table 5.5.

Table 5.5: Young's module for each part of the structure

Part	Young's module (GPa)
Shell panel	30
Plate	38
Truss bar	176
Spar Cap	40-176
Shear Web	176

The buckling load were calculated for eight different values of the Young's modules. The results are shown in Figure 5.6.

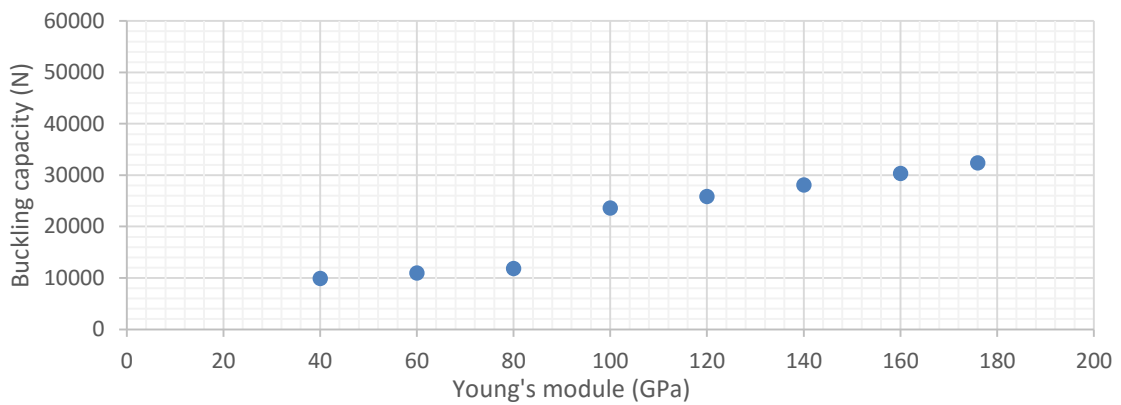


Figure 5.6: Buckling capacity vs. Young's module for spar cap

5.4.1.5 Shear Web

The Young's modulus was changes between 40 and 176 GPa for the spar cap section. The Young's modulus for the rest of the structure are shown in Table 5.6.

Table 5.6: Young's module for each part of the structure

Part	Young's module (GPa)
Shell panel	30
Plate	38
Truss bar	176
Spar Cap	176
Shear Web	30-176

The buckling load were calculated for nine different values of the Young's modules. The results are shown in Figure 5.7.

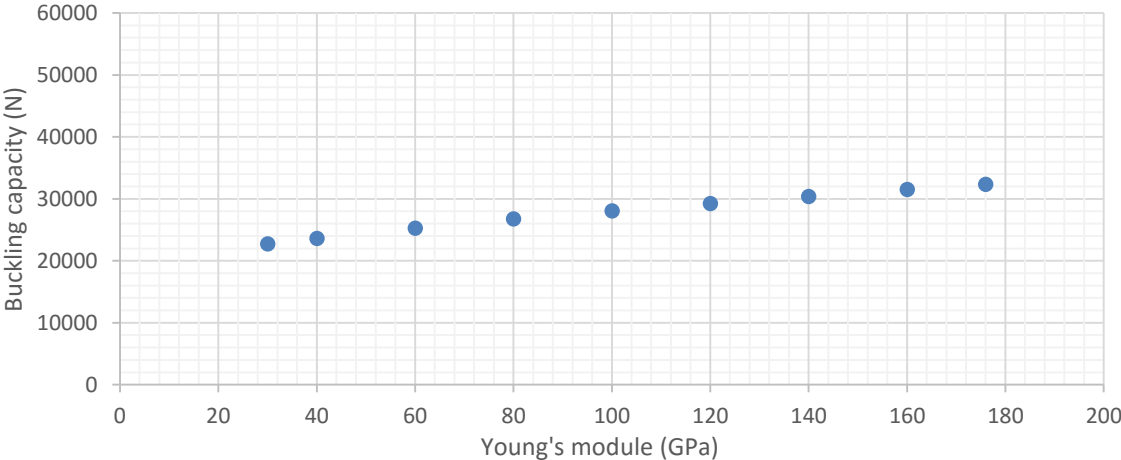


Figure 5.7: Buckling capacity vs. Young's module for shear web

5.4.1.6 Truss bar stiffness

The Young's modulus was changes between 40 and 176 GPa for the spar cap section. The Young's modulus for the rest of the structure are shown in Table 5.7.

Table 5.7: Young's module for each part of the structure

Part	Young's module (GPa)
Shell	30
Plate panel	38
Truss bar	38-176
Spar Cap	176
Shear Web	176

The buckling load were calculated for six different values of the Young's modules. The results are shown in Figure 5.8.

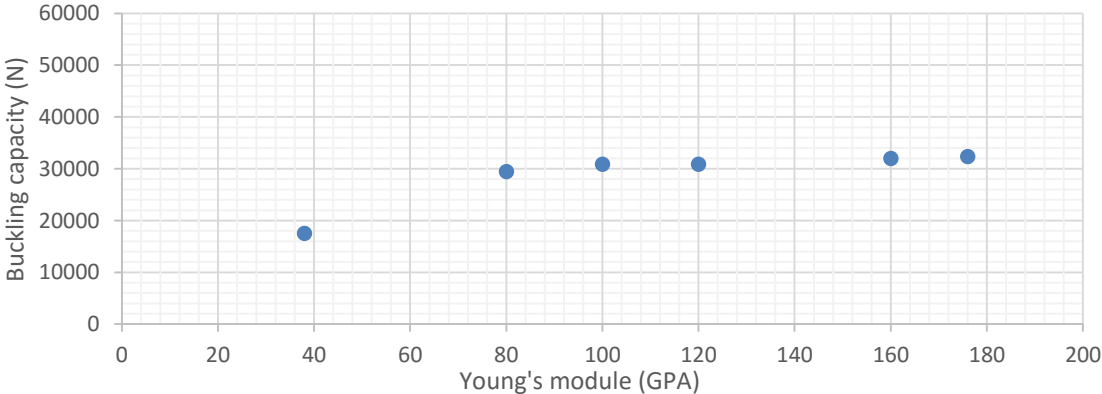


Figure 5.8: Buckling capacity vs. Young's module for truss bar element

5.4.1.7 Conclusions and Choice of Material

Each structure part is assigned the following material:

Shell panel, GFRP. The buckling load capacity is higher for the whole structure when a material with low Young's module is assigned to the shell panels as shown in Figure 5.4. The material chosen for this this section of structure is GFRP since it has a lower Young's module.

For a plate in general the critical buckling stress are linear proportional to Young's module. The critical buckling stress can be written as:

$$\sigma_{crit} = k E t^2 \quad 5.17$$

Where E is Young's module, t is the thickness of the plate and k being a constant depending on the geometry of the plate, Poisson's ratio and boundary conditions of the plate (Bulson, 1970). According to this equation, an increased Young's module is leading to a linear proportional increased critical load.

In this case however are the critical buckling load lower when the Young's module is increased. The reason for this is that an increasing of the Young's module also changes the stress distribution between shell panel and the spar cap. When a low value the Young's module is the stress also decreased in the shell panels instead are the stress in the spar cap increasing. Since the spar cap has a shorter span and is thicker than the shell panel is the value of k higher for the spar cap compared to the shell. Therefore, are the critical buckling stress higher for the spar cap. This leads to in this case to a higher buckling load capacity is reached when the shell panels have a low Young's module.

Plate, GFRP. GFRP is used for this part even though the critical load were significantly higher when a high Young's modulus was used, as shown in Figure 5.4. To increase the capacity of the plate is the shape geometry changed by decreasing the size of the central hole.

Spar cap and shear web, CFRP. These are together creating the box beam that is the primary structural part for each individual blade. They are designed to carry most of the stresses in the structure should therefore be made of a stiffer material like CFRP.

Truss bars, CFRP. As seen in Figure 5.8 are the loading capacity reduce significantly when the module is reduced under 80 MPa . The purpose of the truss bars is to reduce the stresses in blade which is achieved if the truss bars are stiffer.

5.4.2 Section Dimensions

Analyses of varying the section thickness was performed to find with a critical buckling load higher than the load from the CFD analysis. The truss bars and the plates properties is fixed in this analyzes (see Table 5.8). The focus instead is finding the dimensions for the section parts of the blade: spar cap, shell panel and shear web.

Table 5.8: Fixed parameters for section designed

Part	Material	Young's Modulus (GPA)	Poisson's Ratio	Cross section	Shell thickness
Truss bar	CFRP	178	0.3	0.100 x 0.03	-
Plates	GFRP	38	0.3	-	0.03

5.4.2.1 Example of Buckling Mode

An example of a buckling mode from the second parameter study is shown in Figure 5.8.

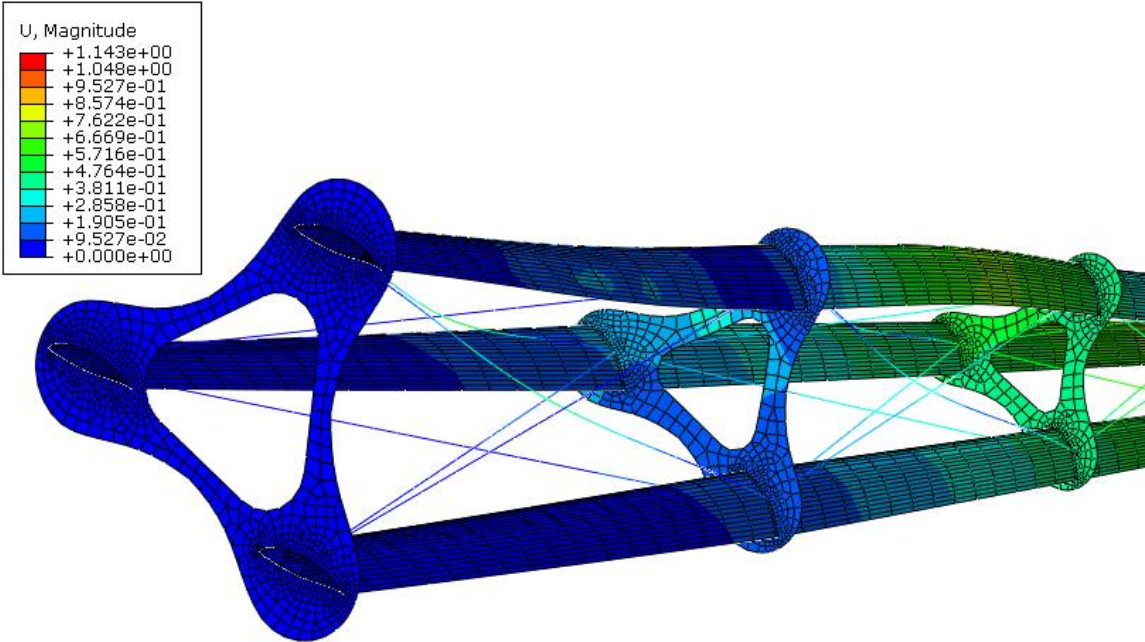


Figure 5.9: Displacements of section 1 and section 2

The buckling of the second plate is shown in Figure 5.9 as well as the load-displacement curve for the tip in Figure 5.10.

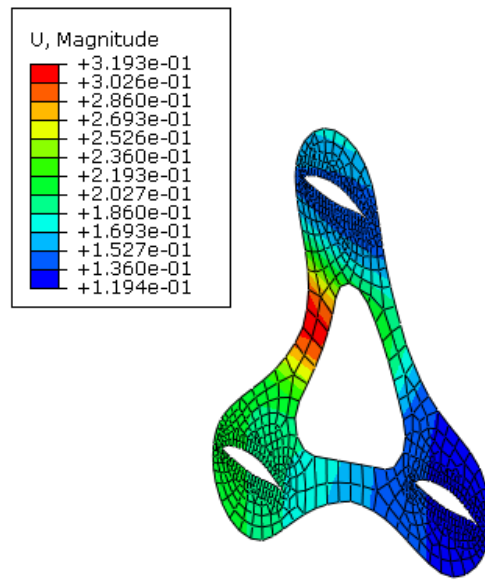


Figure 5.10: Buckling plate

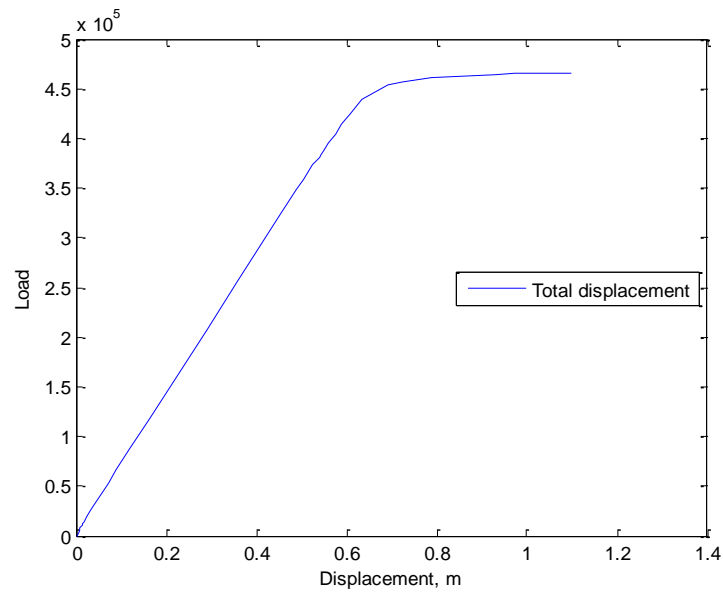


Figure 5.11: Load function of displacement for tip

The tip displacement as well as the von Mises stresses for truss bars in section 1 to 5 are shown in Figure 5.12.

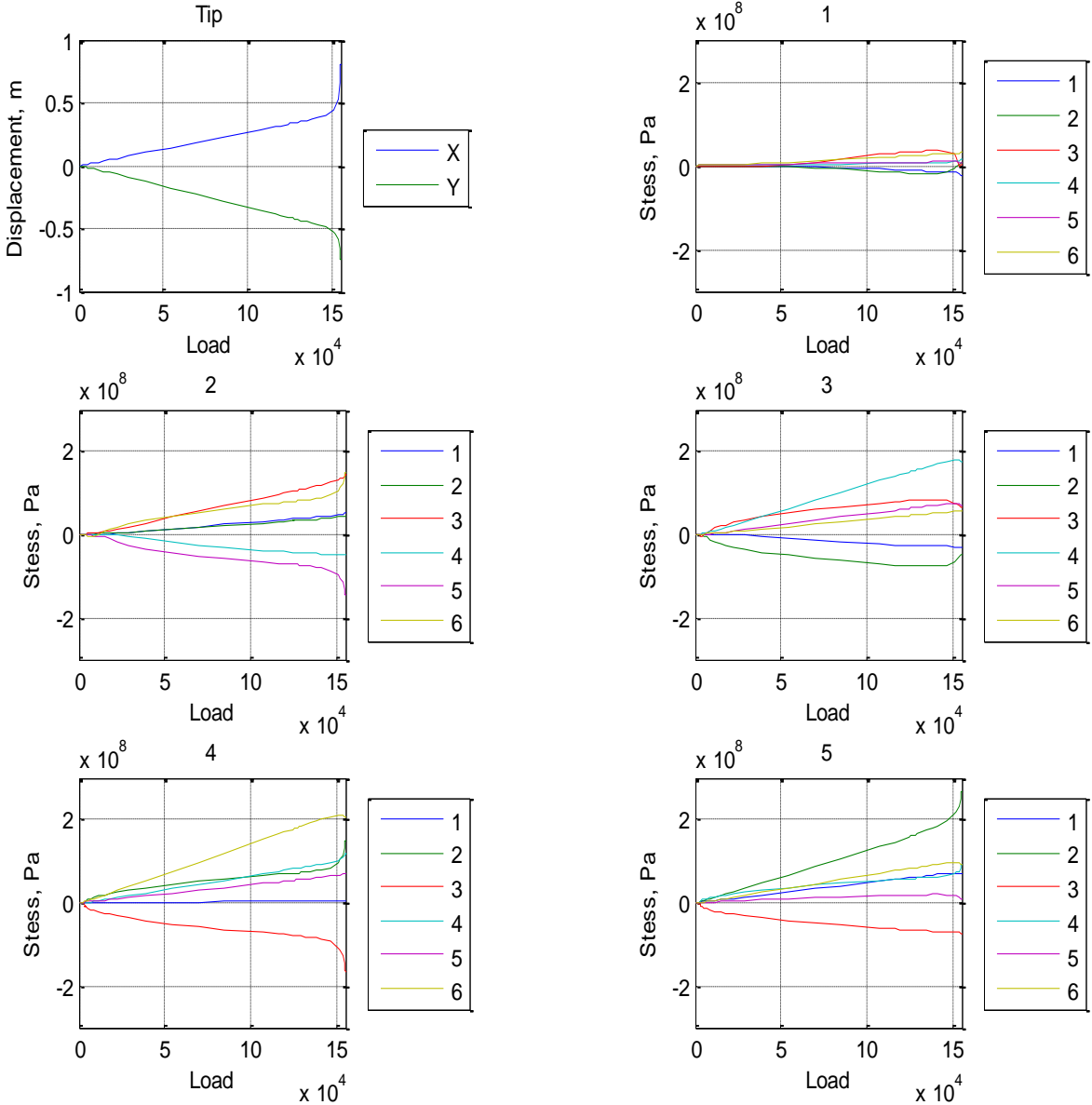


Figure 5.12: Tip displacement and stresses for truss bars in section 1 to 5

5.4.2.2 List of Simulations

The shell thickness for the spar cap, shear web and shell panel will start at 30, 10 and 10 mm respectively. These section thickness is giving a F_{crit} value that is higher than F_{dim} . Each section will then be reduced until the ratio F_{crit}/F_{dim} is just over 1. This process is listed in Table 5.9.

Table 5.9: Calculations made for the section analysis

Shell thickness (m)			Critical load, F_{crit} (kN)	Ratio, F_{crit}/F_{dim}	Buckling mode
Spar cap	Shear Web	Shell			
0.03	0.01	0.01	910	2.42	Bending of lower wing
0.025	0.01	0.01	797	2.12	Bending of lower wing
0.02	0.01	0.01	680	1.81	Bending of lower wing
0.015	0.01	0.01	557	1.48	Bending of lower wing
0.02	0.01	0.008	659	1.76	Bending of lower wing
0.02	0.01	0.006	610	1.63	Bending of lower wing
0.02	0.01	0.004	402	1.07	Buckling of shell
0.02	0.004	0.006	550	1.47	Bending of lower wing
0.02	0.004	0.005	587	1.56	Bending of lower wing
0.015	0.004	0.006	455	1.21	Bending of lower wing
0.015	0.004	0.005	466	1.24	Bending of lower wing
0.014	0.004	0.005	360	0.96	Buckling of shell
0.013	0.004	0.005	350	0.93	Buckling of shell
0.012	0.004	0.005	327	0.87	Buckling of shell
0.014	0.004	0.004	273	0.73	Buckling of shell
0.013	0.004	0.004	262	0.70	Buckling of shell
0.012	0.004	0.004	250	0.67	Buckling of shell

5.4.2.3 Conclusions and Choice of Section dimensions

In this analyses the buckling mode is not identical as in the previous analysis. The mode shape, shown in Figure 5.9, consist of a blade buckling together with a plate. This generates a nonlinear deflection for the whole Triblade (Figure 5.11).

In Figure 5.9 it is also visualized how two truss bars are buckling in the first section due to large compression force. The same phenomenon can be seen in the other sections as well. In the diagrams in Figure 5.12 there are always two truss bars with negative stress. These are the truss bars that are likely to get buckled.

The chosen design is listed in Table 5.10. This design will be used in the future dynamic analysis.

Table 5.10 Section dimensions for all structural parts of the Triblade

Structure part	Shell thickness (m)				Cross- section
	Spar	Web	Shell	Plate	Truss bar
Dimension (m)	0.015	0.004	0.005	0.03	0.1 x 0.03

6 Dynamic analysis

6.1 Chapter Abstract

As the magnitude of the load depends on the wind velocity, are varying wind velocity generate a varying load i.e. a dynamic load. In this chapter are the dynamic response analyses for this varying load.

Three different analysis is made: natural frequencies, frequency response function, and transient dynamic response. Each analysis is completed for two identical models. In the first model the structure was unloaded. In the second the static pressure load was applied to the structure before the analyses are computed.

These analyses are made to evaluate out how the Triblade is responding to a dynamic load. This is of important of investigate high stress variation can causes fatigue damage on the truss bar.

6.2 Objective

Find the quantities from the dynamic response such as the displacement, stresses and critical load frequencies.

6.3 Method

Three different analysis (eigenmodes and eigenfrequencies, full transient dynamic response, and frequency response function) is computed for each model. As mentioned in the abstract two different models are used. The difference is described in the following segment:

Model 1 – No load or deformation is applied before the dynamic analysis is computed. Structural sections dimensions according to Chapter 5.4.2.3

Model 2 – The static load is applied before the dynamic analysis is computed. Structural sections dimensions according to Chapter 5.4.2.3

6.4 Eigenmodes and Eigenfrequencies

The eigenfrequencies for the structure are calculated by solving the eigenvalue problem see Chapter 3.3.1. Some example of different eigenmodes are shown in Figure 6.1-6.5. Two different models are used as mentioned previously. The result from the first model is shown in chapter 6.4.1 and the result from the second is shown in chapter 6.4.2.

6.4.1 Results Eigenfrequencies Undeformed Model

The vibrations modes between 0 and 5.2 Hz are listed in Table 6.1. Since the truss bars within each section almost have the same length and have the same cross-section does this lead to that the value of the eigenfrequencies almost being the same. For that reason, are the frequencies for the truss bars listed as in intervals in Table 6.1.

Table 6.1: Eigenfrequencies from 0 to 5.2Hz

Frequencies (Hz)	Part	Vibration mode
1.0257 – 1.0507	Truss bars section in 1	First bending mode
1.4968 – 1.5514	Truss bars section in 2	First bending mode
2.1487	Whole Triblade	First bending mode
2.2546 – 2.3227	Truss bars section in 3	First bending mode
2.4038	Whole Triblade	First bending mode
2.48040	Whole Triblade	First bending mode
2.8329 – 2.8968	Truss bars section in 1	Second Bending mode
3.1324 – 3.2726	Truss bars section in 1	Fist bending mode
3.4290 – 3.5273	Truss bars section in 4	First bending mode
4.3736	Whole Triblade	First twisting mode
4.9071 – 5.2001	Truss section in 5	First bending mode

Five example of eigenmodes from table 6.1 are shown in the following segment.

1.0507 Hz

First natural vibration bending mode of truss bars in section 1.

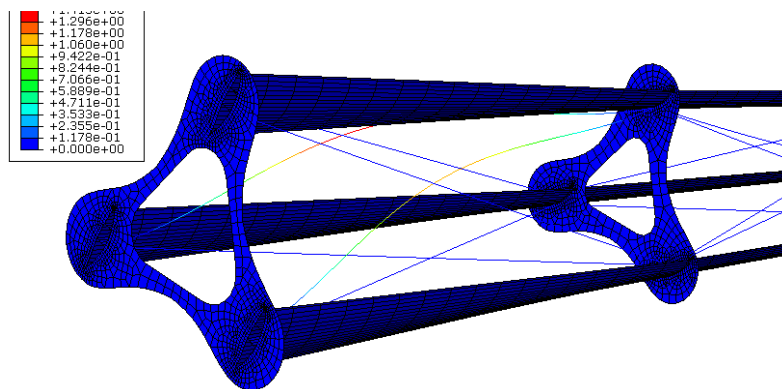
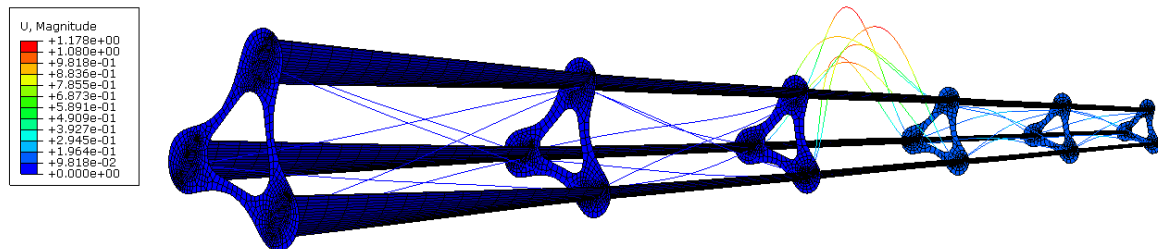


Figure 6.1: First natural bending mode of truss bars

2.1487 Hz

First natural bending mode of a Triblade. The eigenfrequency of this mode is in a close range of the frequency of the first natural vibration mode of truss bars in section 3. This creates large deflection in these truss bars as well. In Figure 6.2b is it clearer that the mode shape is a bending mode of the whole Triblade.



Step: Step-5
Mode 13: Value = 182.27 Freq = 2.1487 (cycles/time)
Primary Var: U, Magnitude
Deformed Var: U Deformation Scale Factor: +5.000e+00

Figure 6.2a: Side view of first natural bending mode of the Triblade

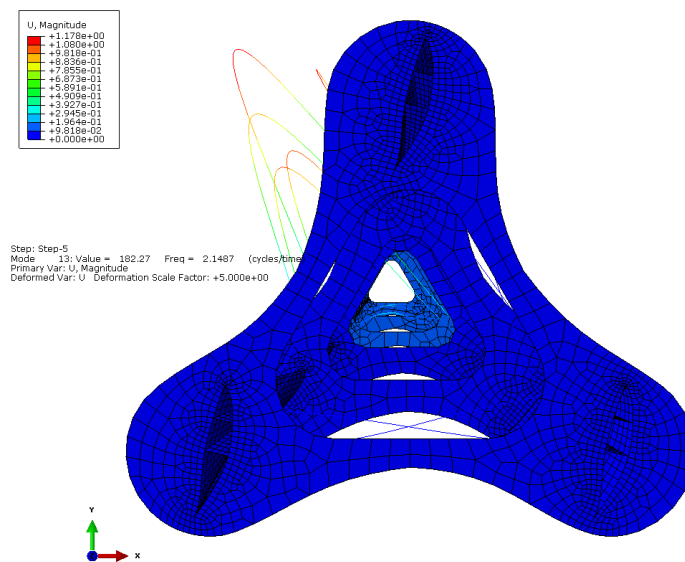


Figure 6.3b: Front view of first natural bending mode of the Triblade

2.4038 Hz

First natural bending mode of Triblade in another direction compared to the mode at 2.1487 Hz are shown in Figure 6.3.

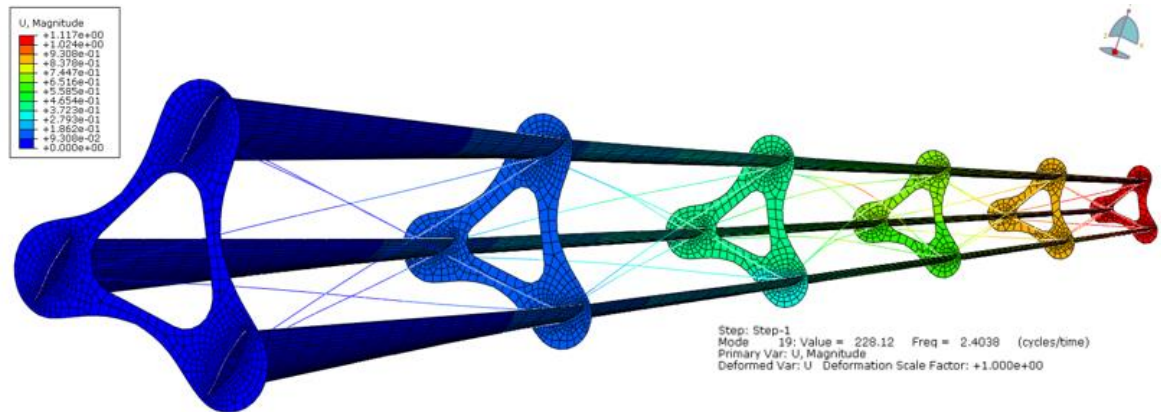


Figure 6.4a: Side view of first natural bending mode of the Triblade

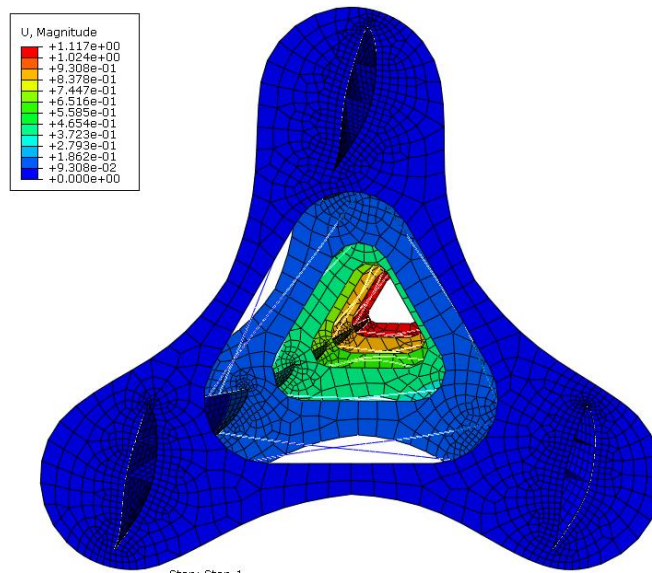


Figure 6.5b: Front view of first natural bending mode of the Triblade

2.4804 Hz

First bending mode of Triblade in the third direction are shown in Figure 6.4.

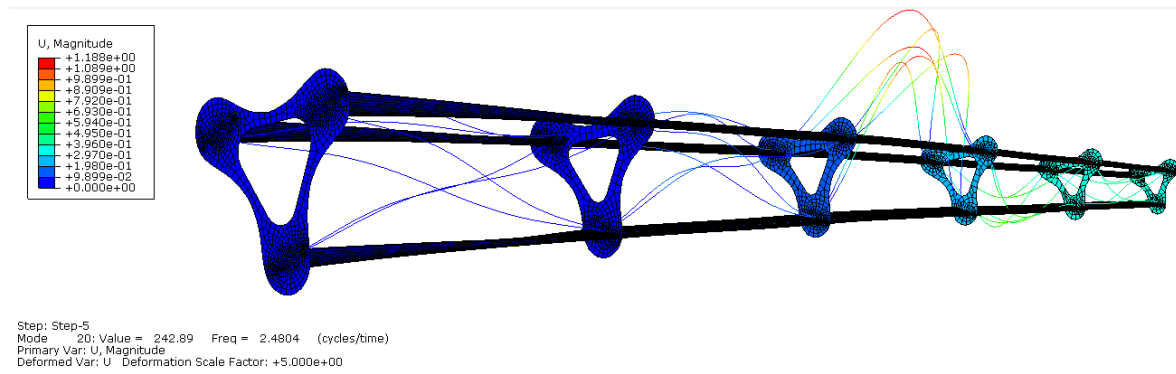


Figure 6.6a: Side view of first natural bending mode of the Triblade

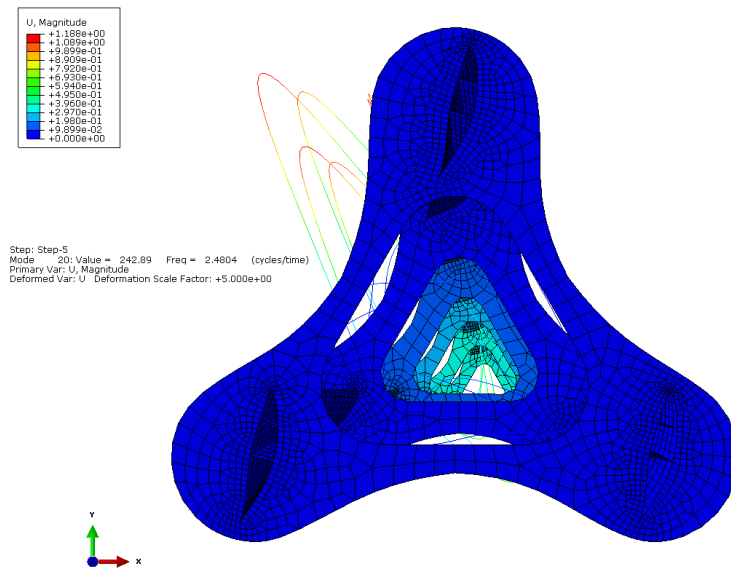


Figure 6.7: Front view of first natural bending mode of the Triblade

4.3736 Hz

The first twisting vibration mode of Triblade are shown in Figure 6.5.

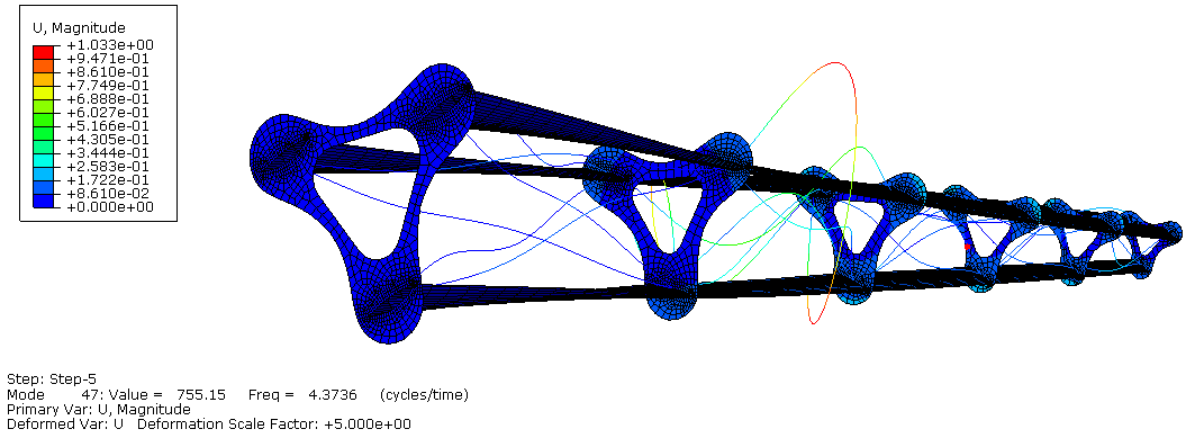


Figure 6.8a: Side view of first twisting mode of the Triblade

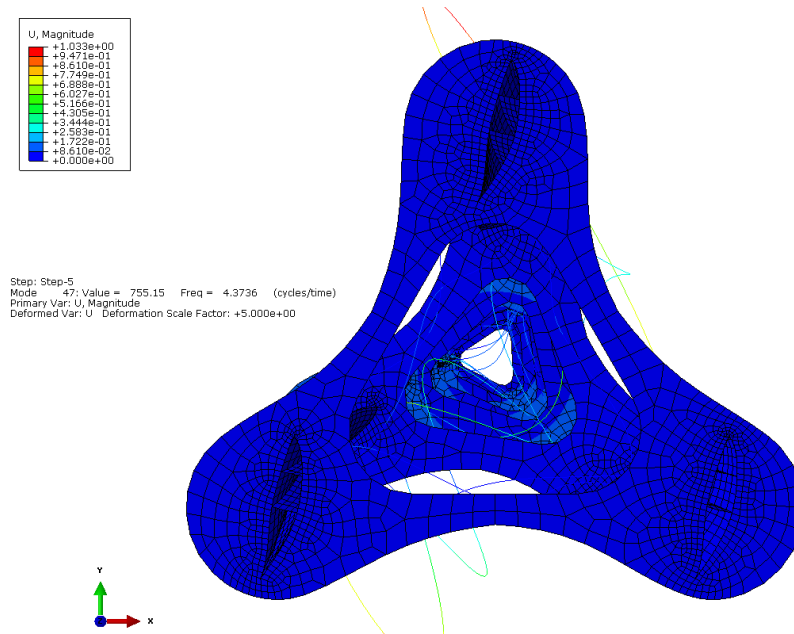


Figure 6.9: Front view of first twisting mode of the Triblade

6.4.2 Results Model 2 Pre-loaded Structure

The eigenmodes between 0 and 4.5 Hz are listed in Table 6.2 along with a description of which part of the Triblade has the highest deflection for each mode. The following abridgement are used: s1 - section one. Some of the modes are shown in the Figures 6.6- Figure 6.10 below the table.

Table 6.2: Eigenfrequencies from 0 to 4.14Hz

Frequency (Hz)	Structural Part	Natural Vibration Mode
0	Buckled truss bars*	First bending mode
2.00869	Whole blade	First bending mode
2.3351	Whole blade	First bending mode
2.60153	Truss bar in s1	First bending mode
2.80943	Truss bar in s1	First bending mode
3.01288	Truss bar in s1	First bending mode
3.22914	Whole blade	Twisting
3.7864	Single blade	First multi support
3.84178	Truss bars s1,s3, s5	First bending mode
3.93933	Truss bar in s1	First bending mode
3.95011	Truss bar in s2	First bending mode
4.09597	Truss bar s3,s5	First bending mode
4.16526	Truss bar in s5	First bending mode
4.32303	Plate 2	First bending mode
4.36766	Truss bar in s2	First bending mode

**In section 1: truss bar 3 and 4. Section 2: truss bar 2 and truss bar 3. Section 3: truss bar 3.*

Five example of eigenmodes from table 6.2 are shown in the following segment on the next page.

2.00869 Hz – First bending mode of Triblade

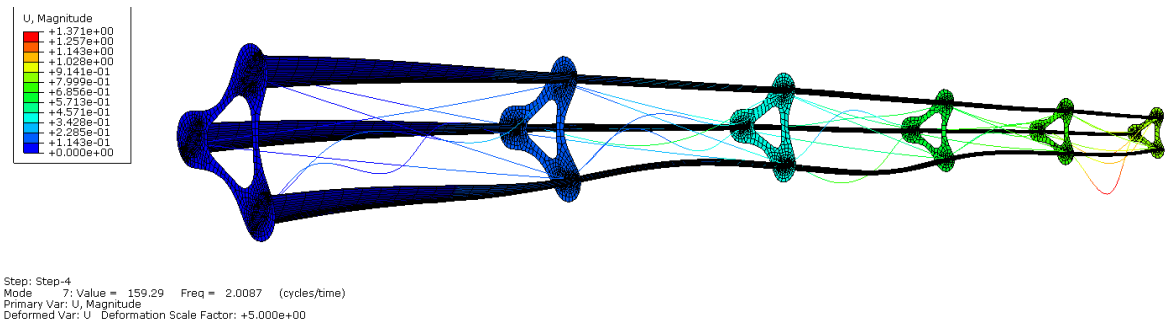


Figure 6.10a: Side view of first bending mode of Triblade

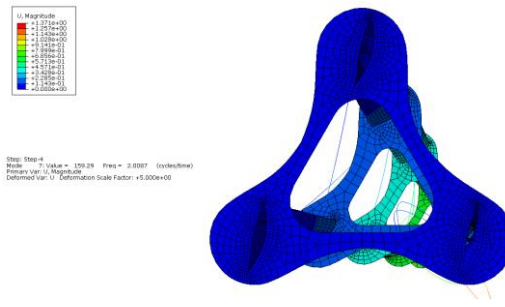


Figure 6.11b: Front view of first bending mode of Triblade

2.3351 Hz – First bending mode of Triblade

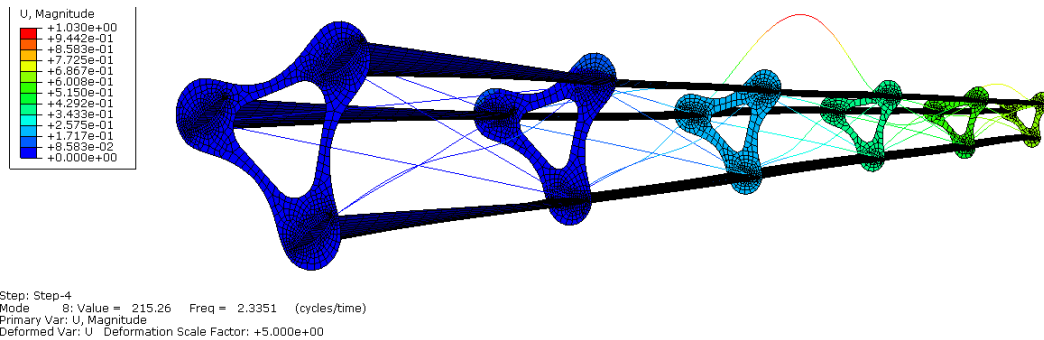


Figure 6.12a: Side view of first bending mode of Triblade

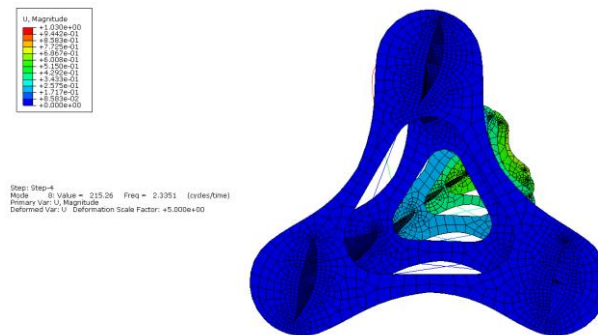


Figure 6.13b: Bending mode of Triblade

3.22914 Hz – First twisting mode of Triblade

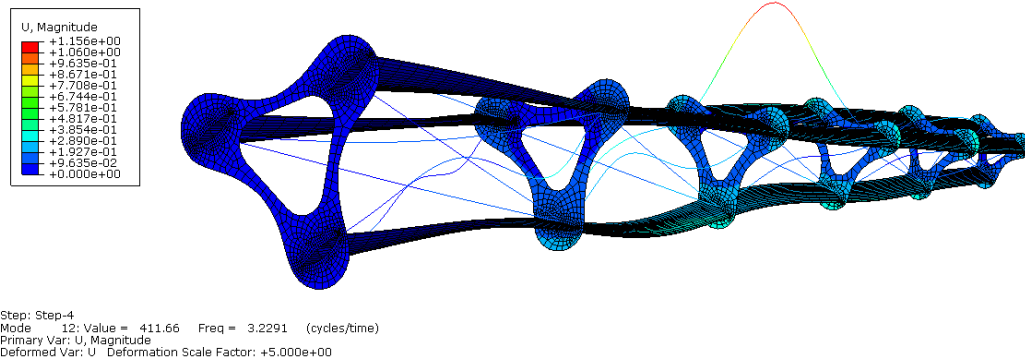


Figure 6.14: Twisting mode of Triblade

3.7864 Hz – Natural vibration mode single blade

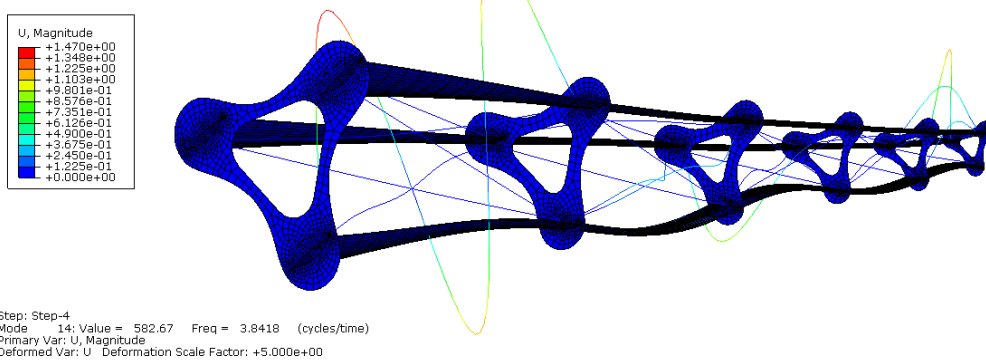


Figure 6.15: Natural Vibration mode blade

4.4429 Hz – First natural vibration mode of plate 2.

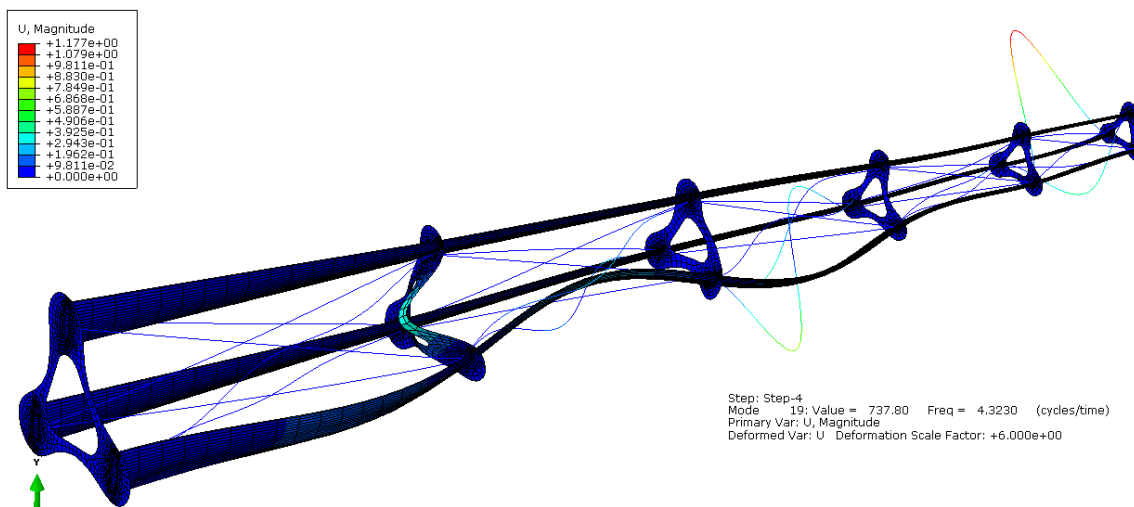


Figure 6.16: First Natural Vibration Mode of plate 2

6.4.3 Conclusions – Modal Analysis

Both analysis gives the first bending mode in the range from 2 Hz to 2.48 Hz. A structure with a high stiffness compared to mass will have higher eigenfrequency than a structure with lower stiffness (Chopra, 2009). The undeformed Triblade (model 1) has higher frequencies, than the deformed Triblade (model 2). This indicate that the stiffness of the deformed blade is lower, which is expected.

The frequency of the truss bars is varying greatly as the eigenfrequency is depending on the normal force in each truss. In the undeformed model there are no forces acting on any of the truss bars, leading to all truss bars within each section does almost have the same eigenfrequency. For the deformed model are some of the truss bars in compression and some in tension which leads to higher variation of eigenfrequencies within each section. In five truss bars are the vibration frequency 0 Hz, this indicates that they have zero stiffness and are therefore buckling.

The truss bars with 0 Hz eigenfrequency will vibrate a lot when an impulse is added to the structure, more about this will be discussed in full transient dynamic response analysis in chapter 6.6.3.

6.5 Frequency Response Function

The FTF are calculates by recoding the response for a periotic load over a series of different frequencies see chapter 3.3.3. The periotic load has the same magnitude and distribution as in the static analysis.

The response is calculated between 0.01Hz and 20Hz. Two different model, one undeformed model and one deformed model are analyzed as mentioned in 6.3. The damping ratio was set to 2% of critical damping.

The result from the frequency response analysis are shown in chapter 6.5.1 respective 6.5.2.

6.5.1 Results Model 1 – Undeformed Model

The tip deformation vs frequency curve is shown in Figure 6.11 for the vertical (u1) and horizontal (u2) deformation. In Figure 6.12 - 6.16 the stress variation for all struts within each section are shown.

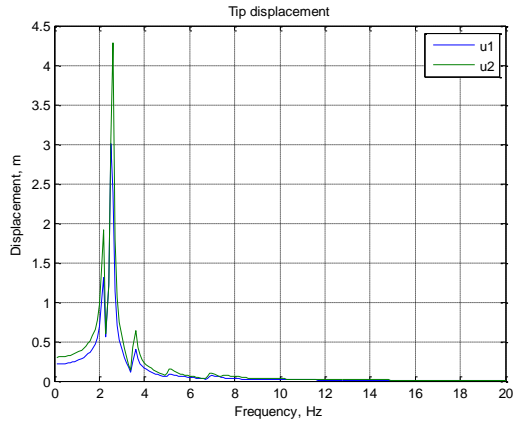


Figure 6.17: Tip displacement

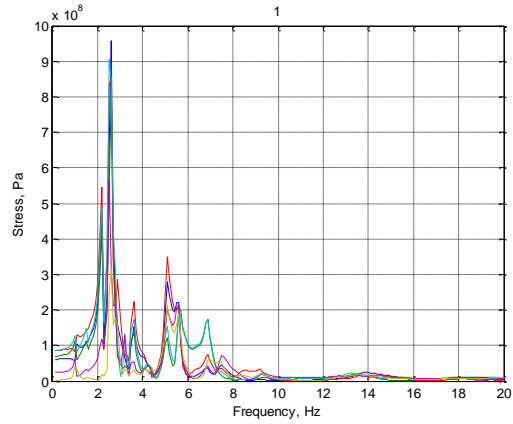


Figure 6.18: Stresses in truss bar in section 1

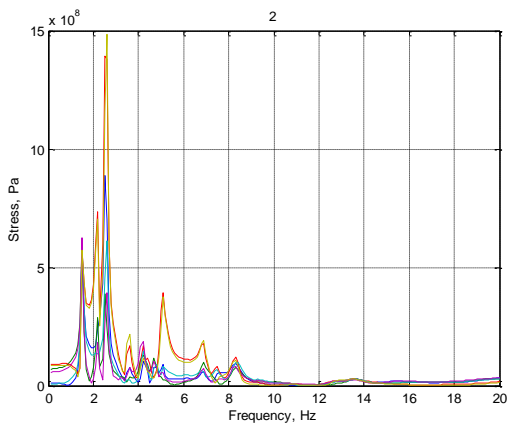


Figure 6.19: Stresses in truss bar in section 2

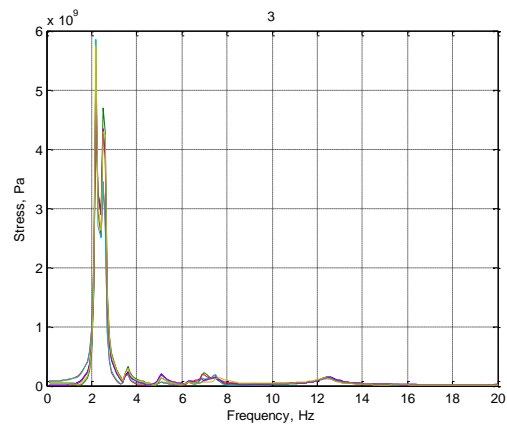


Figure 6.20: Stresses in truss bar in section 3

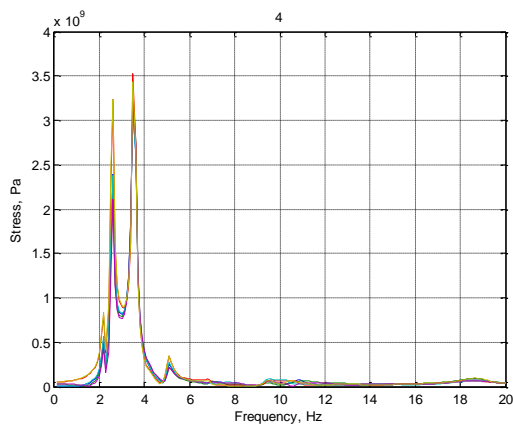


Figure 6.21: Stresses in truss bar in section 4

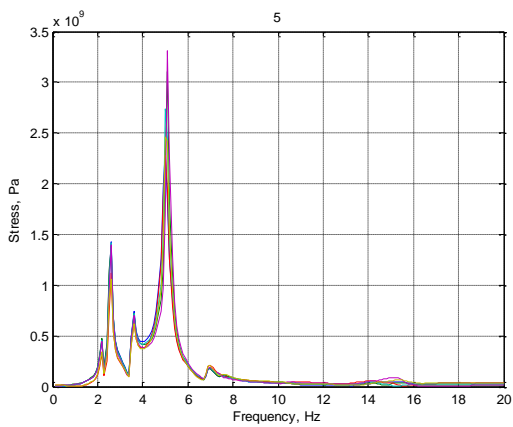


Figure 6.22: Stresses in truss bar in section 5

6.5.2 Results Model 2 – Deformed model

The tip deformation vs frequency curve is shown in Figure 6.17 in the wind direction (X) and the rotation direction (Y). In Figure 6.18 - 6.22 are the stress variation for all struts within each section shown.

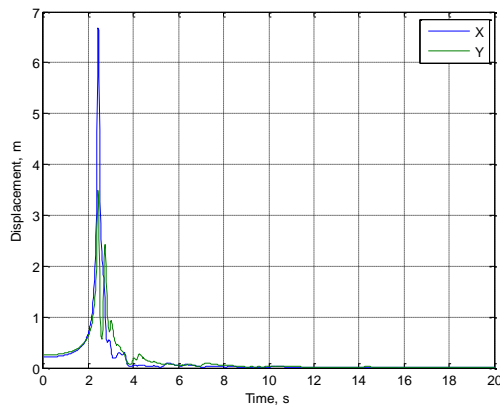


Figure 6.23: Tip displacement

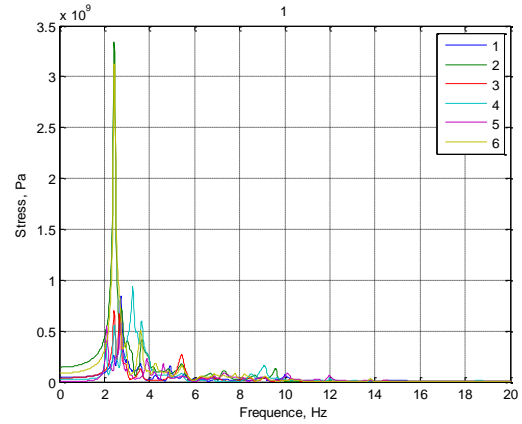


Figure 6.24: Stresses in truss bar in section 1

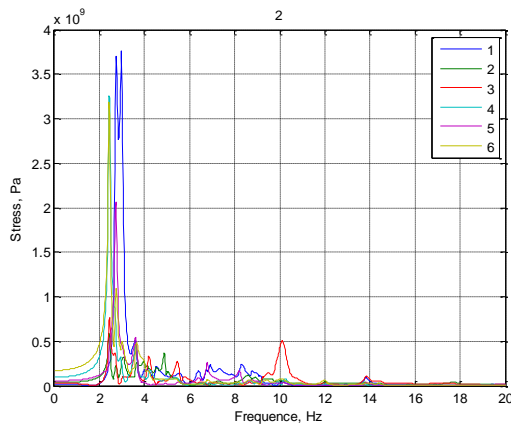


Figure 6.25: Stresses in truss bar in section 2

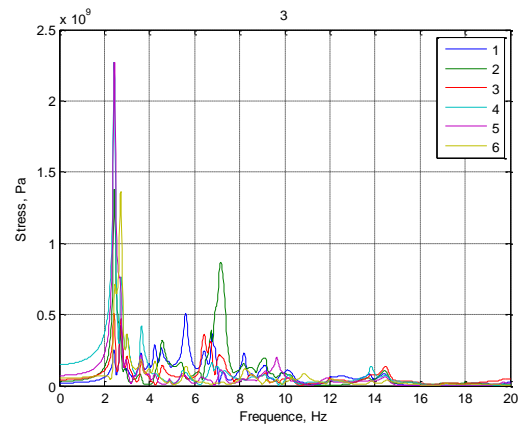


Figure 6.26: Stresses in truss bar in section 3

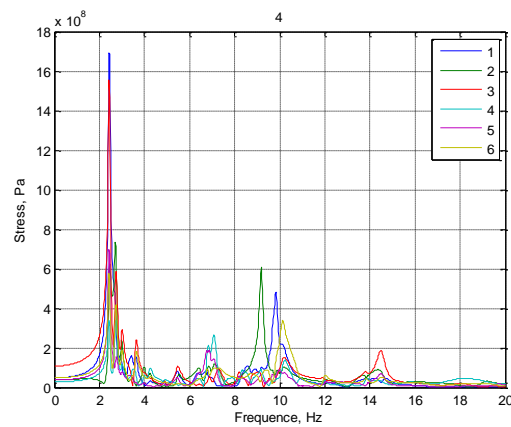


Figure 6.27: Stresses in truss bar in section 4

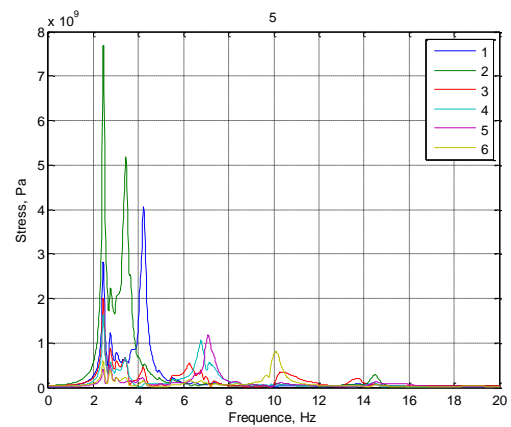


Figure 6.28: Stresses in truss bar in section 5

6.5.3 Conclusions

The FRF of the structure is calculated from a load applied in the model with a known magnitude and distribution. The FRF gives therefore a better understanding of which vibration modes that are activated when a certain load is applied. In a modal analysis no such load is used.

Comparing the displacement/stress diagrams between the two different models one can see that there is not a lot of difference in the results. Both the highest tip deformation and highest stress in almost every truss bar is occurring at around 2 Hz. This is the frequency of the first natural vibration mode for the Triblade that was calculated in the modal analysis.

Additionally, to the maxima at 2 Hz do the truss bars have at least one more maxima which is at the same frequency as that truss bars eigenfrequency. If this eigenfrequency has approximately the same frequency as the 2 Hz Triblade leads this to high stresses as can be seen in Figure and 6.14. This is the reason why section 3 is producing the highest stresses. A conclusion is therefore that in the future development of the Triblade should it be avoided that the eigenfrequencies of a truss bars should not have the same value as the bending eigenfrequencies of the whole Triblade.

6.6 Full Transient Dynamic Response

The transient dynamic response is calculated using implicit time integration see Chapter 3.3.2. The load input in this equation is dynamic load that were approximated in Chapter 4.6. The applied impulse are approximately 0.08 times higher compared to the static load. The response is calculated over 10 seconds. The damping ratio was set to 2% of critical damping.

Two different model, one undeformed model and one deformed model are analyzed as mentioned in 6.3.

The impulse for the unloaded structure is shown in Figure 6.23.

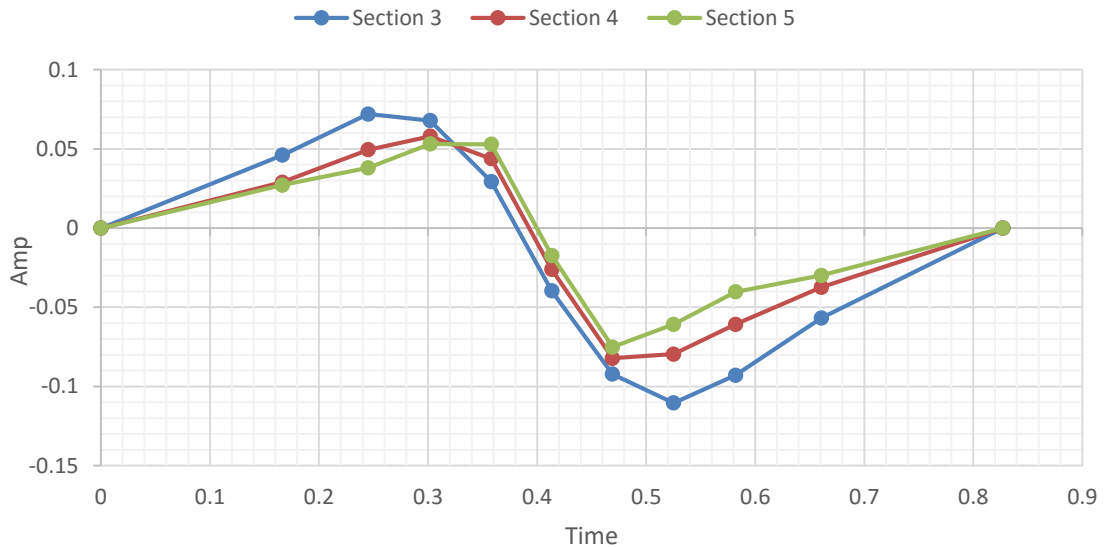


Figure 6.29: Amplitude in time added to create an impulse to an unloaded structure

Since the deformed model already are loaded are a different impulse added to this structure

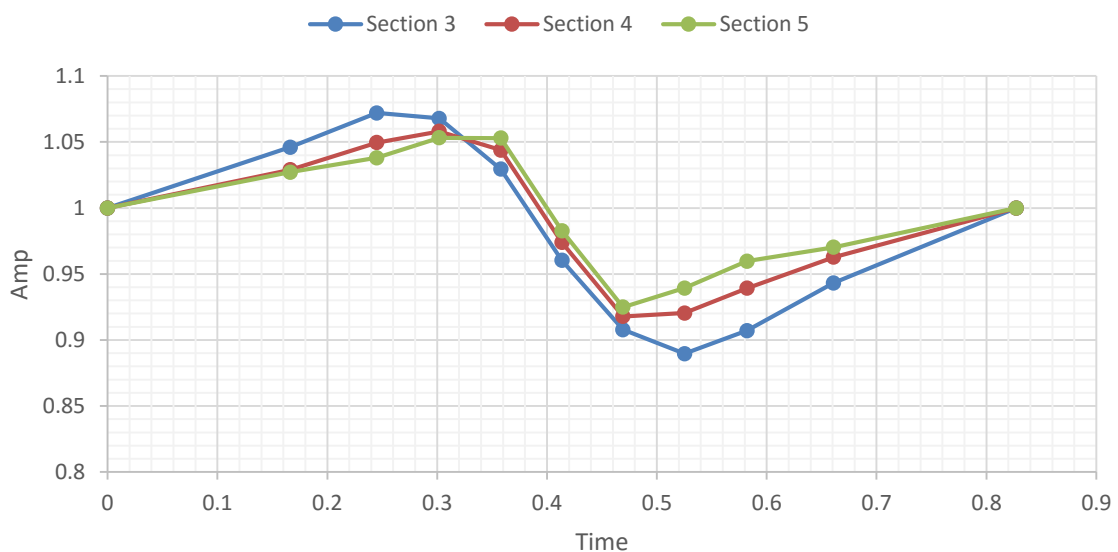


Figure 6.30: Amplitude in time added to create an impulse to a loaded structure

6.6.1 Full transient Dynamic Response

The first Figure 6.25 are the tip deflection over time shown. In Figure 6.26-6.30 are the stress over time for the truss bars each section shown. The top diagram in these figures are showing the stresses over time for all truss bars in that section, the one in bottom is just showing the stress diagram of the truss bar with the highest stress amplitude.

6.6.2 Model 1 – Undeformed Model

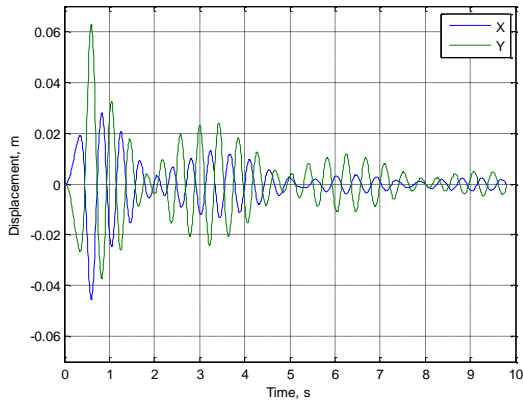


Figure 6.31: Tip displacement

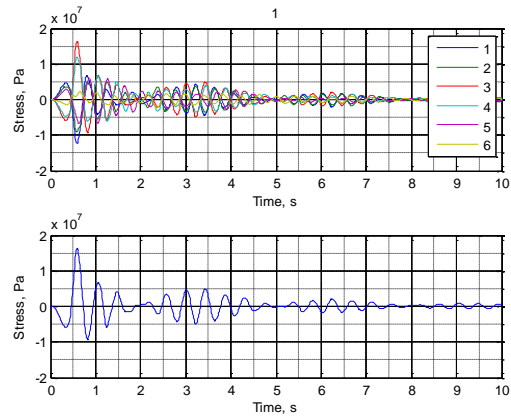


Figure 6.32: Stresses in truss bars in section 1

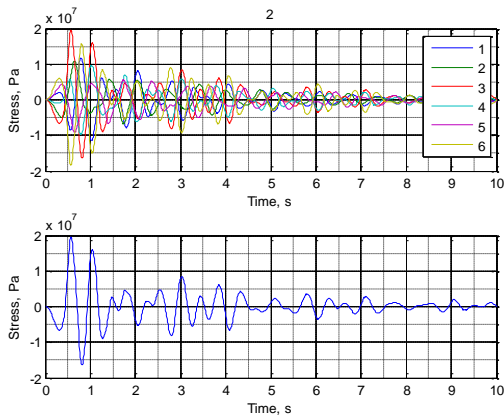


Figure 6.33: Stresses in truss bars in section 2

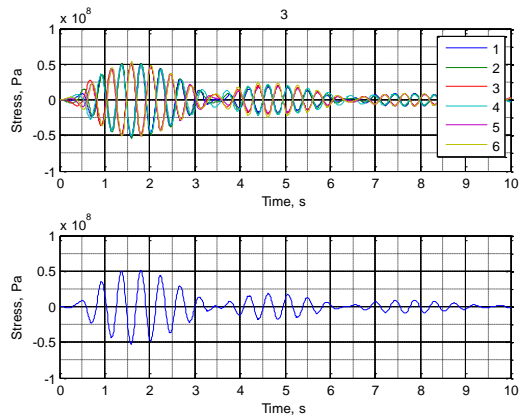


Figure 6.34: Stresses in truss bars in section 3

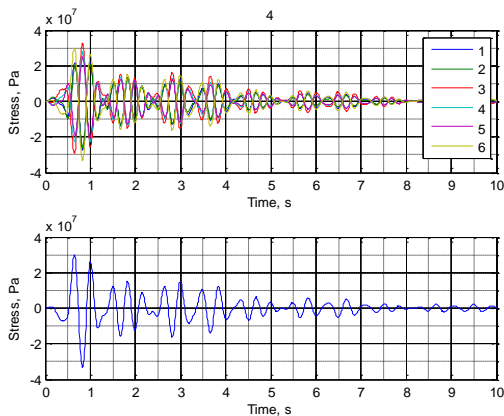


Figure 6.35: Stresses in truss bars in section 4

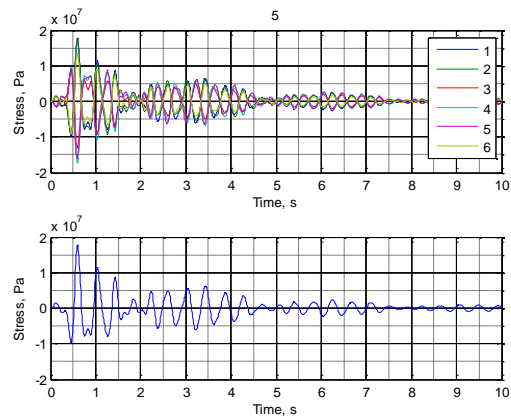


Figure 6.36: Stresses in truss bars in section 5

6.6.3 Model 2 – Deformed Model

The first Figure 6.31 the tip deflection is shown over time. In Figure 6.31-6.36 are the stresses over time for each section shown.

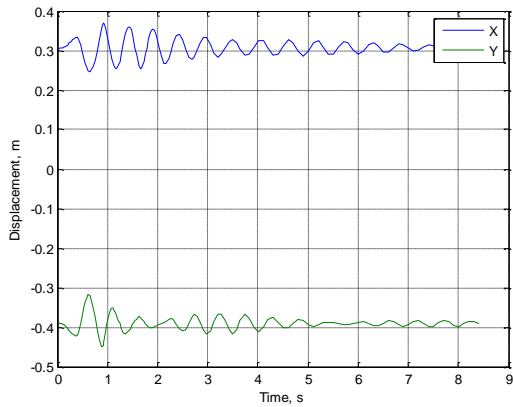


Figure 6.37: Tip displacement

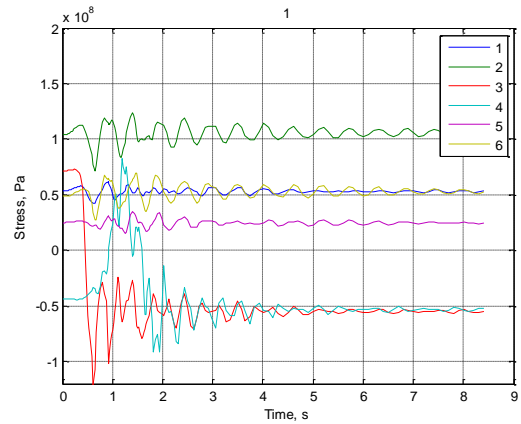


Figure 6.38: Stresses in truss bars in section 1

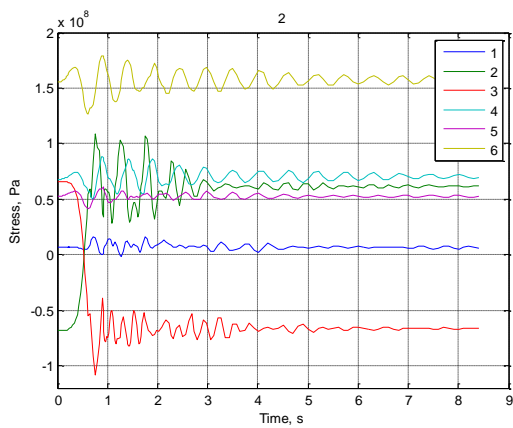


Figure 6.39: Stresses in truss bars in section 2

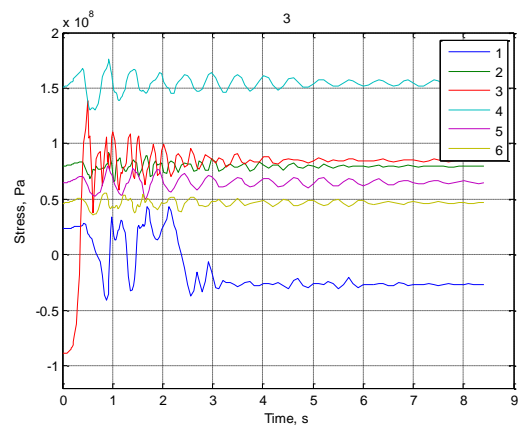


Figure 6.40: Stresses in truss bars in section 3

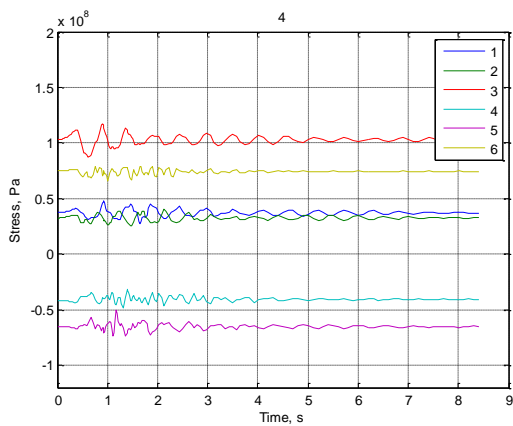


Figure 6.41: Stresses in truss bars in section 4

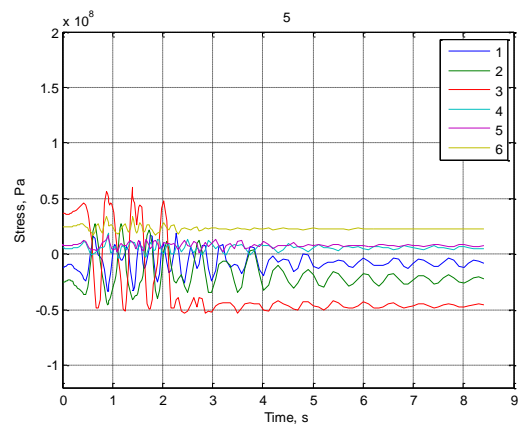


Figure 6.42: Stresses in truss bars in section 5

6.6.4 Conclusions

In the analysis of the undeformed model are the Triblade vibrating in two slightly different frequencies. This creates a beat frequency. This phenomenon is most apparent in section 3 (Figure 6.23) and tip deformation (Figure 6.20). A beat frequency is creating a minimum when the two wave frequencies are 180 degrees out of phase. The maximum of one wave frequency is at this phase canceled out by the other wave frequencies minimum. When the two frequencies are in phase are the maximum of both of the frequencies summed up. In section 3 is this effect producing stresses that are much higher than the stress during the impulse. The highest stress is generated after approximately 1.8sec compared to the impulse having the highest load at 0.8 sec. This effect can be avoided by making sure the natural frequency of the Triblade is not overlapping with the natural frequency of the truss bar as already mentioned in 6.4.3.

In the analysis of the deformed structure is the effect of adding an impulse to an already buckled truss bar shown. Adding an impulse to the structure causes the buckled truss bars to deform in another buckling mode compared to the original mode. Figure 6.43 is visualizing the original buckling modes and Figure 6.44 is visualizing the buckling modes after the impulse. The change of buckling mode is the reason to why the stress variation for some bars starts at one level and ends at another level (see Figure 6.28, Figure 6.29, Figure 6.30 and Figure 6.32). A large variation of stresses causes the truss bars to take fatigue damage, which is decrease the bars life span of that truss bars and should therefore be avoided.

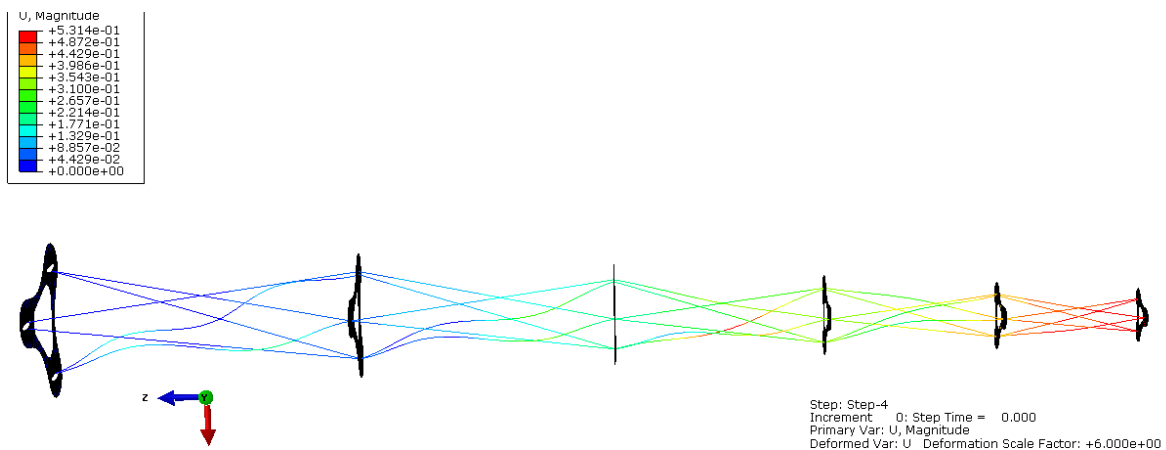


Figure 6.43: Truss bars buckling mode at $t = 0$ seconds

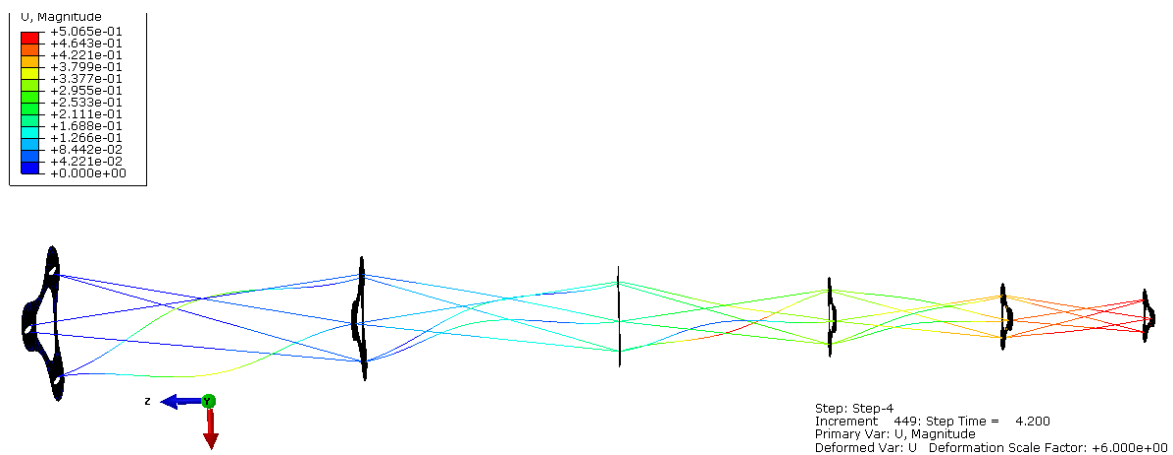


Figure 6.44 Truss bars buckling mode at $t = 4.2$ seconds

7 Discussion and Future Work

Other analyses have been made during the work of this theses than has been mentioned in this report. As an example of this is a linear buckling analysis. This was made to compare with the nonlinear buckling capacity. Due to the low buckling capacity of a single truss bars where almost every buckling modes different mode shapes of a single truss bar buckling. Finding a buckling mode that would correspond to global buckling capacity would be very hard to find.

A similar problem also occurred in the modal analysis. It is difficult to see if a modal shape is a global mode or a local truss bar. By first creating, a FRF is easy to see which frequencies are creating the highest deformation and stresses and from this results it's easier to find the eigenmodes of the whole structure.

The results presented in this report came from Abaqus models and no laboratory testing has been performed. To evaluate that the truss structure system works as intended in the models, laboratory testing has to be conducted. A proposal for further work is therefore construct a Triblade by first scaling down the Triblade in size and decreasing the amount of sections. A laboratory test can be performed to investigate if the behavior is similar to the FE model.

Some simplifications have been made in this model. For example, are the materials simplified by being isotropic. Some improvements of the model can be made by modeling the model in more realistic materials:

- Instead of modeling the shell panels and shear web as shell elements of either CFRP or GFRP, could be modeled as sandwiching material since these is most commonly used in the wind turbine blades.
- The CFRP and GFRP is model as elastic isotropic material. These materials are in reality orthotropic with higher stiffness in the fiber direction. A suggestion for further work would be to investigate the material properties further to improve the model.
- All contact between the different parts are model as fixed contacts. A thin layer of adhesive could be used instead between the plates and blades.

A conclusion from this thesis are that the buckling truss bars has poor performance when an impulse is applied to the structure. The further investigations should focus on reducing the compression force in these truss bars. A possible alternative would be to investigate the effect of removing the truss bars that are in compression since the truss bars are not increasing the static load capacity of structure when it is loaded in the main load direction.

8 References

- Bortolotti, Pietro (2012). Carbon Glass Hybrid Materials for Wind Turbine Rotor Blades
- Brøndsted, Povl & Lilholt, Hans & Lystrup Aage (2005). Composite Materials for Wind Power Turbine Blades. Roskilde: Annual Reviews
- Bulson P. S., Theory of Flat Plates (1970) , London, Chatto and Windus.
- Chopra, Anill K. (1995). DYNAMICS OF STRUCTURES, New Jersey: Prentice Hall
- Cook, Robert D. & Malkus David S. & Plesha, Michael E. & Witt, Robert J. Concepts and Applications of Finite Element Analysis. New York, John Wiley & Sons. Inc.
- Dassault Systèmes SIMULIA (2013). Abaqus 6.11 Documentation, Daussault Systèmes Inc S.A, <http://abaqus.ethz.ch:2080/v6.11/>, visited 2015-06-23
- Gómez, Alejandro & Seume, Joerg R. (2009). Aerodynamic Coupling of Rotor and Tower in HAWTs, Hannover: Leibniz University Hannover
- International Electrotechnical Commission (1999). Wind Turbine Generator Systems – Part 1: Safety Requirements. 2nd edition, International standard
- Söker, H. (2013). Advances in wind turbine blade design and materials, Chapter 2, Philadelphia: Woodhead Publishing Limited
- Ottosen & Petersson (1992). Introduction to the Finite Element Method, Lund: Prentice Hall
- Devriendt, Christof & Weijtjens, Wout (2015). The overall damping of an offshore wind turbine during different operating conditions.